Materials Horizons

ROYAL SOCIETY OF CHEMISTRY

REVIEW

View Article Online
View Journal | View Issue

Cite this: *Mater. Horiz.*, 2024, **11**, 6289

Customized surface adhesive and wettability properties of conformal electronic devices

Wenfu Chen,[a] Junzhu Lin,[a] Zhicheng Ye,[a] Xiangyu Wang,[ab] Jie Shen[c] and Ben Wang*[a]

Conformal and body-adaptive electronics have revolutionized the way we interact with technology, ushering in a new era of wearable devices that can seamlessly integrate with our daily lives. However, the inherent mismatch between artificially synthesized materials and biological tissues (caused by irregular skin fold, skin hair, sweat, and skin grease) needs to be addressed, which can be realized using body-adaptive electronics by rational design of their surface adhesive and wettability properties. Over the past few decades, various approaches have been developed to enhance the conformability and adaptability of bioelectronics by (i) increasing flexibility and reducing device thickness, (ii) improving the adhesion and wettability between bioelectronics and biological interfaces, and (iii) refining the integration process with biological systems. Successful development of a conformal and body-adaptive electronic device requires comprehensive consideration of all three aspects. This review starts with the design strategies of conformal electronics with different surface adhesive and wettability properties. A series of conformal and body-adaptive electronics used in the human body under both dry and wet conditions are systematically discussed. Finally, the current challenges and critical perspectives are summarized, focusing on promising directions such as telemedicine, mobile health, point-of-care diagnostics, and human–machine interface applications.

Received 13th June 2024,
Accepted 23rd August 2024

DOI: 10.1039/d4mh00753k

rsc.li/materials-horizons

Wider impact

Recent research on flexible electronic devices has focused on preparation technology, mechanical performance control, and bioelectronic applications. However, current reviews lack a systematic summary of key characteristics such as adhesion and wettability. This paper explores progress in surface wetting and adhesion control to ensure long-term stability and adaptability in wet or underwater environments. We describe the application strategy of flexible electronics in interface contact, summarize essential performance characteristics, and discuss the different signal types relevant to detecting human health. Additionally, we systematically review the applications of flexible electronics in the human body and *in vivo* under various adhesion and wetting conditions, address current challenges, and propose feasible countermeasures. The future development trends, including waterproof, breathable, and wet adhesion applications, are also discussed. We hope this review will guide researchers in advancing flexible electronics for biodegradable diagnostics, point-to-point diagnostics, and human–machine interfaces.

1 Introduction

Traditional electronic devices are fabricated using metal- or metal-derivative-based conductive elements deposited on thick, inflexible substrates and are attached to the surface of the human body through external auxiliary devices.[1–14] The changes in the mechanical signals caused by human physiological reactions or skin deformation during body movements are then converted into electronic signals, such as capacitance and resistance, to realize real-time monitoring. Traditional electronic sensors are often rigid and fragile and have poor contact with conformal skin,[15–28] resulting in a poor usage experience and unstable signals.[29,30]

Soft and flexible electronics offer distinct advantages for integration of multiple functions with exceptional mechanical and biological compatibilities. These advantages include (1) enhanced mechanical durability of the devices, (2) the ability to conformingly interact with bio-tissues or establish three-

[a] *College of Chemistry and Environmental Engineering, Shenzhen University, Shenzhen 518055, P. R. China. E-mail: benwang@szu.edu.cn*
[b] *State Key Laboratory of Featured Metal Materials and Life-cycle Safety for Composite Structures, MOE Key Laboratory of New Processing Technology for Nonferrous Metals and Materials, and School of Resources, Environment and Materials, Guangxi University, Nanning 530004, P. R. China*
[c] *Shenzhen Key Laboratory of Spine Surgery, Department of Spine Surgery, Peking University Shenzhen Hospital, Shenzhen 518036, P. R. China*

dimensional connections, (3) reduced mechanical interference with bio-systems, and (4) long-term compatibility with biological systems. Flexible electronics are ideal devices capable of delivering mechanical and electrical stimulations to

Wenfu Chen

Wenfu Chen joined Prof. Wang's group at Shenzhen University in 2022 to pursue his PhD degree. His research primarily investigates interface sensing within the field of soft robotics, with a focus on developing sensors that can dynamically adapt to varying interfaces, providing real-time, high-precision feedback to enhance the functionality and responsiveness of soft robotic systems.

Junzhu Lin

Junzhu Lin is currently an undergraduate at the College of Chemistry and Environmental Engineering, Shenzhen University. His main research direction is the soft robots for the gastrointestinal tract.

Zhicheng Ye

Zhicheng Ye received her BS degree from the College of Chemistry and Environmental Engineering at Shenzhen University, in June 2024. After graduation, she joined Professor Zhang Li's research group in the Department of Mechanical and Automation Engineering at The Chinese University of Hong Kong as a research assistant. Her research is centered on the imaging and targeted delivery of micro/nanorobots, focusing on developing advanced techniques for precise and efficient drug delivery systems.

Xiangyu Wang

Xiangyu Wang earned his master's degree from the School of Resources, Environment, and Materials at Guangxi University. His research primarily revolves around the biomimetic fabrication of micro-nanostructured materials and the development of environmental energy harvesting devices.

Jie Shen

Jie Shen received his PhD degree from the University of Hong Kong in 2018. Then, he successively worked as a postdoctoral fellow at the University of Hong Kong and as an assistant professor and an associate professor at the Peking University Shenzhen Hospital. His main research areas are functional biomaterials and tissue regeneration.

Ben Wang

Ben Wang received his PhD from the Department of Biomedical Engineering at The Chinese University of Hong Kong (CUHK). Following his doctoral studies, he served as a postdoctoral fellow in the Department of Mechanical and Automation Engineering at CUHK, where he was part of the Impact Postdoctoral Fellowship Scheme. In December 2019, he joined Shenzhen University as an assistant professor. His research primarily explores the development of bioinspired soft robots, emphasizing their applications in remote actuation and targeted delivery. He has published over 80 SCI-cited papers, including Sci. Robot., Sci. Adv., with more than 5800 citations.

produce quantitative electrical signals.[31–37] Biological integrated electronic devices can be thinner, softer, and more flexible and are thus suitable for establishing a conformal interface with the human skin. These features improve the wearing experience, signal detection, and treatment efficiency of integrated devices, allowing them to outperform traditional diagnostic instruments or wrist-mounted wearable devices. As a result, portable integrated electronic devices can facilitate accurate healthcare monitoring, disease diagnosis, and seamless human–computer interactions.[38–46]

However, it is worth noting that the practical applications of these flexible and wearable electronic products for long-term use must take into account the integrity and sensitivity changes of the devices,[47–50] including various hydration conditions of both the environment (external) and the human body (internal).[51–53] External environmental factors include exposure to rain and bathing, while internal factors include sweat and lipid secretion from the skin. Accumulation of water molecules inside flexible electronic devices or prolonged exposure to water on their surfaces can lead to bacterial contamination. Sweat secreted during motion monitoring using flexible electronics cannot be expelled from the body's surface, leading to corrosion of devices and batteries, decreased sensitivity, poor wearing comfort, and potential safety risks.[54,55] To address this challenge, constructing hydrophobic and hydrophilic surfaces on flexible electronic surfaces using capillary force to expel sweat from the body can extend the lifespan of flexible electronic devices.[54]

In recent years, researchers have effectively adjusted the wetting properties between the surface of flexible electronics and liquids during their construction, enabling their extensive application under different hydration conditions.[55] Examples include waterproof wearable devices, sweat sensors,[56,57] underwater swimming sensors,[58] contact lenses,[59] blood flow and pressure monitoring sensors,[60] and internal sutures for surgery.[61] Additionally, encountering hydrated environments during prolonged use can also reduce the adhesion strength at the device/interface. Therefore, the consistency between the external and internal interfaces of the human body and flexible electronic surfaces has also been widely studied. When flexible electronics come into close contact with the skin interface, their sensitivity improves significantly, but their performance can be influenced by interface factors such as skin folds and hair growth on the skin. Researchers can enhance the adhesion of flexible electronics to the skin interface through material selection and structural design. By reducing device thickness and adopting biomimetic structural designs, flexible electronics can find a wide range of applications both externally and internally in the human body, including surgical masks with sensors,[62,63] wound dressing sensors,[64] electromyographic (EMG) monitoring sensors,[65,66] electroencephalographic (EEG) monitoring sensors[67] and human–machine interaction with electronic tattoos,[68] as shown in Fig. 1.

Recent reviews on flexible electronics have mainly focused on preparation techniques, mechanical performance control, and their applications as integrated bioelectronic devices.[75–78] While these reviews offer a fundamental understanding of the latest developments in flexible electronics across interdisciplinary fields, this review aims to discuss progress from the perspective of surface wetting and adhesion control to ensure the long-term stability and adaptability of flexible electronics in humid or underwater environments (Section 1). Starting with strategies for designing consistent electronic devices, we delve into adhesiveness, categorizing it into dry adhesion and wet adhesion. We further discuss surface wetting from the perspective of surface modification and the construction of micro/nano-bioinspired structures, concluding with different structures of materials (Section 2). Next, we introduce the performance characteristics that flexible electronics should possess (Section 3). Subsequently, we discuss different types of signals monitored using wearable electronic devices adhered to the body, as well as the manifestations of different signals (Section 4). Specifically, based on the application areas of different surface adhesion and wetting conditions on the human body, we systematically summarize the applications of consistent and adaptable electronics, including on-body and in-body applications (Section 5). Finally, we summarize the current challenges and key perspectives (Section 6), with a focus on directions such as electronic health, mobile health, point-to-point diagnosis, and human–machine interface applications.

2 Design strategies of conformal electronics for the human body

In people's daily lives, wearable electronic devices have become indispensable in the field of healthcare.[20,79] These devices capture physiological and biochemical signals from the human body in real-time and portably, providing valuable health information directly to the wearer.[80,81] Ensuring that these devices adhere closely to the skin is crucial for improving the accuracy and stability of monitoring signals. However, factors such as hair, sebum, and the varying external moisture environment often pose challenges to the adhesion of wearable electronic devices.[82,83] Therefore, continuously exploring and innovating design strategies to overcome these practical application challenges is particularly important. To address the aforementioned issues, a series of carefully planned strategies have been developed, focusing on four core areas: optimization of dry adhesion mechanisms, innovation in wet adhesion technologies, precise regulation of wettability treatment, and in-depth optimization of material structure and composition. In terms of adhesion strategies, we particularly focus on effectively dealing with the interference of hair and sebum to ensure secure and comfortable contact between the device and the skin. Meanwhile, managing wettability is equally crucial because sweat after exercise, water flow during showers, and moisture in daily activities can all impact device performance. By designing innovative surfaces that rapidly drain liquids or by coating advanced hydrophobic materials, we can precisely regulate the wettability environment of the material, maintaining its optimal working state. Additionally, the selection of materials and structural design are key elements in enhancing both adhesion and wettability. The materials we carefully select must not only possess excellent biocompatibility and durability

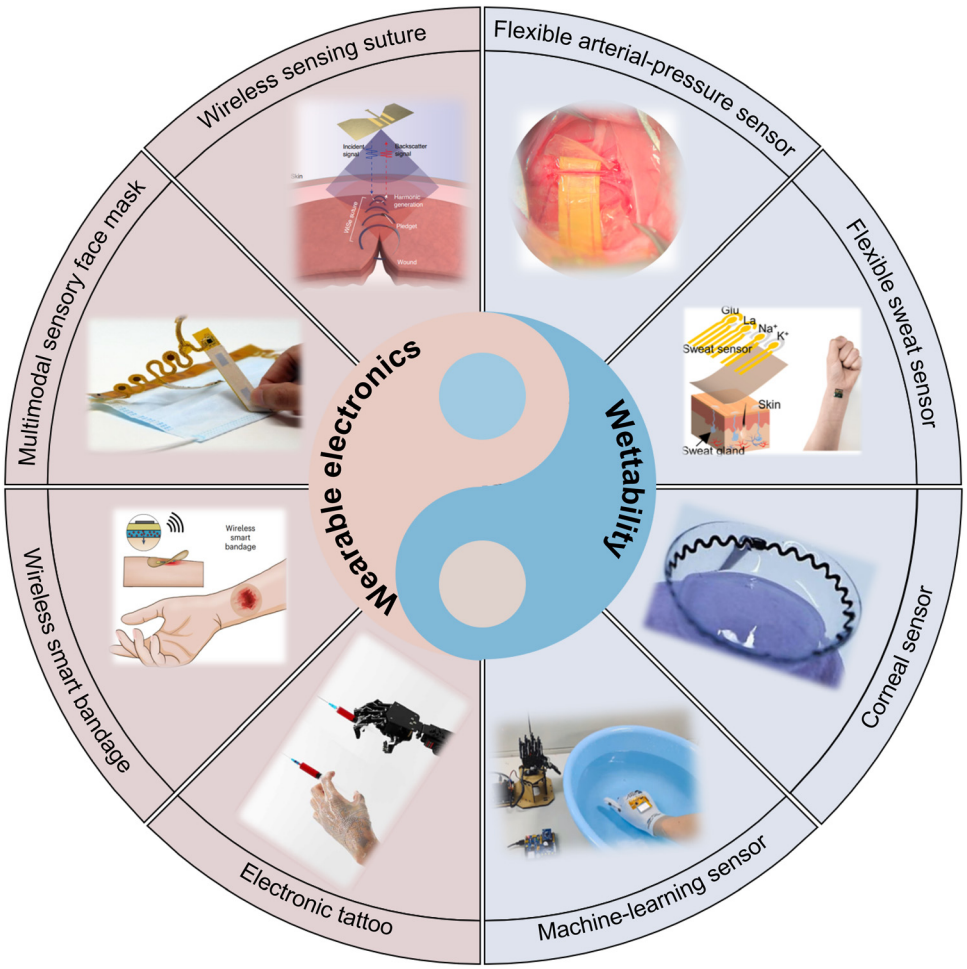

Fig. 1 Schematic illustration of the applications of wettable wearable electronics. Image of a "Wireless sensing suture": adapted with permission under a Creative Commons CC BY License from ref. 61. Copyright 2021 The Authors, published by Springer Nature. Image of a "Multimodal sensory face mask": adapted with permission under a Creative Commons CC BY License from ref. 69. Copyright 2022 The Authors, published by Springer Nature. Image of a "Wireless smart bandage": adapted with permission under a Creative Commons CC BY License from ref. 70. Copyright 2022 The Authors, published by Springer Nature. Image of "Electronic tattoo": reproduced under terms of the Creative Commons Attribution 4.0 International License from ref. 71. Copyright 2021 The Authors, published by American Association for the Advancement of Science. Image of a "Flexible arterial-pressure sensor": adapted with permission under a Creative Commons CC BY License from ref. 60. Copyright 2021 The Authors, published by Elsevier. Image of a "Flexible sweat sensor": reprinted (adapted) with permission from ref. 72. Copyright 2022, American Chemical Society. Image of a "Corneal sensor": adapted with permission under a Creative Commons Attribution 4.0 International License from ref. 73. Copyright 2021 The Authors, published by Springer Nature. Image of a "Machine-learning sensor": reproduced with permission from ref. 74. Copyright 2021, Elsevier.

but also exhibit stable adhesive properties under various environmental conditions. Through optimizing structural design, we can further enhance these properties, ensuring that wearable electronic devices can provide accurate and reliable health monitoring services in various scenarios. By comprehensively employing advanced strategies in dry adhesion, wet adhesion, and wettability treatments and material structure design, it is possible to develop wearable electronic devices that effectively address practical application challenges. This will drive the development of these devices towards higher levels of functionalities, such as waterproofing, self-cleaning, and high sensitivity.

2.1 Adhesion

It is well known that the surface of human skin is made up of complex structures, with rough textures visible on fingerprints, wrinkles, creases and pits on the face.[84,85] This complexity poses a challenge to the effective application of traditional rigid electronic devices to skin texture structures.[86,87] Thus, the emergence of wearable electronics allows them to establish conformal contact with the rough, wet, hairy, curvy and textured surfaces of human skin, which is essential for obtaining high-quality bio-signals.[88] In response to different usage scenarios, adhesion can be categorized into dry adhesion and wet adhesion according to the requirements of the usage scenario. Dry and wet adhesion design strategies and the advantages and disadvantages of applications are summarized in Table 1.

2.1.1 Dry adhesion. Reducing the thickness of wearable electronic devices can effectively enhance their adhesion to the skin and mechanical flexibility.[96,97] Fujie *et al.*[98] reported that by reducing the thickness of the device to several hundred

Table 1 Dry and wet adhesion design strategies and advantages and disadvantages of applications

Application scenario	Strategies	Advantages	Limitations	Ref.
Dry adhesion	Ultrathin film	High frequency performance and low power consumption	Achieving bendable and flexible devices is more challenging	89
	Nanomesh	Excellent mechanical robustness, high skin adhesion, breathability, and anti-drying properties	High manufacturing technology and operational challenges	90
	Hydrogel	Highly efficient, self-reinforcing and long-lasting interfacial adhesion	Unadhered interfaces tend to harden, toughen, and lose adhesiveness	91
	Tattoos	Flexible and stretchable, with a modulus similar to human tissue, causing no damage	Cannot simultaneously achieve joining, conforming to creases, and being multilayered	71
	Microstructure	Provides strong, reversible adhesion adaptable to various non-flat surfaces	Susceptible to skin hair growth and thicker	92
Wet adhesion	Wet compatibility factor	Self-regulating adhesion	Additional processing steps increase operational complexity and affect production efficiency	93
	Bioadhesives	Enhanced adhesion by chemical bonding	Low bond strength, poor dynamic reversibility, weak environmental resistance	94
	Microstructure	Reusability and reduction of external pressure	Applying to soft, non-flat skin poses challenges	95

nanometers, strong adhesiveness to the human body can be achieved without the need for external fixation methods. This design enables wearable flexible electronic products to effectively adhere to dry skin surfaces, laying a solid foundation for their application in specific usage scenarios. Therefore, it is necessary to flexibly choose the structure and type of materials according to the application scenarios of wearable devices, allowing them to form good contact with interfaces under dry conditions. To achieve better adhesion between wearable devices and interfaces under dry conditions, the materials can be designed in the form of ultra-thin films, tattoos, nano-network structures, and microstructures, which can effectively achieve better interface adhesion through surface treatment. Additionally, different material types can provide design ideas for wearable devices, such as hydrogels and carbon-based materials. Using the thin and light characteristics of electronic tattoos, graphene electronic tattoos can be designed to control their thickness, which is 463 ± 30 nm, and can be directly laminated onto human skin. The graphene layers stacked together in the electronic tattoo form graphite, maintained by van der Waals forces between the layers. Thus, the seamless fit between the graphene electronic tattoo and the skin interface is achieved through van der Waals forces (Fig. 2a).[99] To improve the comfort and breathability of wearable devices, those designed with nano-network structures can enhance adhesion to the skin surface by increasing surface roughness and effective contact area, maintaining this adhesion over time. The increased contact area of the nano-network structure provides good breathability, helps reduce the risk of inflammation related to wearable electronic devices on the skin surface, and improves wearer comfort (Fig. 2b).[47] Hydrogels, with their softness and high hydration properties, can adapt to any surface to form interface adhesion and improve adhesive strength. Chemical modification or functionalization of hydrogels can adjust their surface hydrophilicity or hydrophobicity to suit dry adhesion environments. Additionally, the high fatigue resistance of hydrogels provides strong mechanical performance for the design of wearable electronic devices. Liu *et al.*[100] created ion-crosslinked hydrogel skin using ionic and covalent crosslinking and bio-adhesives. This hydrogel skin has strong surface adhesion, firmly adhering to the skin even under dry conditions, adapting to complex skin structures, and providing high breathability to prevent skin irritation (Fig. 2c). To meet adhesion assurance needs while ensuring multifunctionality, electronic tattoos are created using a layer-by-layer method to achieve wrinkle amplification. Moreover, these electronic tattoos do not require external treatments such as solvents or heating when transferred to different surfaces, allowing them to firmly adhere to the skin surface. To improve wearer comfort, wearable devices are designed as textiles for better breathability (Fig. 2d).[71] Microfluidic sensors integrated into fabrics utilize the characteristics of hollow microchannel structures to minimize the contact area with the skin, addressing the challenges of poor breathability and comfort of wearable electronic products. For better reversible adhesion on specific surfaces, many biological microstructures, such as micropillars, microcavities, or microgrooves, have inspired designs in nature. These structural features help enhance adhesion performance on complex surfaces and under dry conditions. Wearable electronic products designed based on these unique biological microstructures closely adhere to the human skin interface and provide reversible adhesion, extending the lifespan of wearable devices. Wearable devices made by simulating micro-hair interface structures establish seamless conformal adhesive contact with the irregular surface of the skin (Fig. 2e).[101] Furthermore, by designing and regulating microstructures, the hydrophilicity or hydrophobicity of the material's surface can be controlled to achieve adhesion under dry conditions. Increasing the roughness and effective contact area of the microstructure surface can improve the adhesion between the material and the interface.

2.1.2 Wet adhesion. The wet adhesion of wearable devices refers to their ability to effectively adhere to surfaces in the presence of sweat, oil secretions, and external humid environments, thereby extending the lifespan of wearable electronics in everyday use. Establishing an environment that accommodates the wet interface between wearable devices and the human body is crucial. To enhance the wet adhesion of wearable

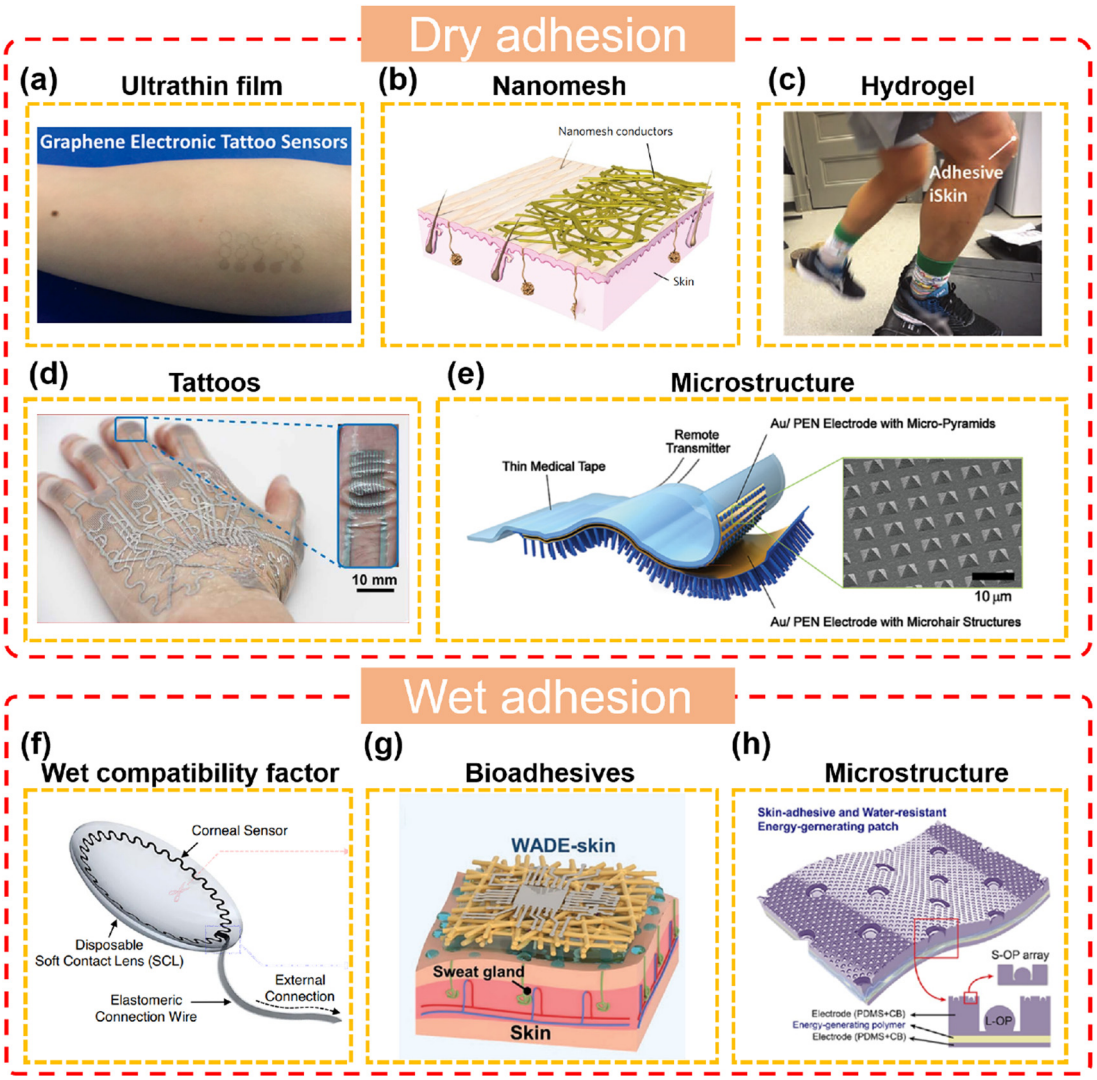

Fig. 2 Schematic illustration of dry adhesion and wet adhesion. (a) Nano-graphene tattoos with reduced device thickness adhere to the surface of the skin. Reprinted (adapted) with permission from ref. 99. Copyright 2017, American Chemical Society. (b) Stretchable skin electronics with nanomesh exhibit high conformability and adhesion to the skin. Reproduced with permission from ref. 47. Copyright 2017, Springer Nature. (c) Conceptual setup of a hydrogel adhered to the knee for gait measurement, demonstrating good adhesion capability. Reproduced with permission from ref. 100. Copyright 2021, John Wiley and Sons. (d) Multilayer tattoos adhered to dry skin, capable of embedding optical images into creases of the finger joints. Reproduced under terms of the Creative Commons Attribution 4.0 International License from ref. 71. Copyright 2021 The Authors, published by American Association for the Advancement of Science. (e) Cross-sectional diagram of a microstructured sensor improving conformal contact with the skin. Reproduced with permission from ref. 101. Copyright 2014, John Wiley and Sons. (f) Schematic diagram of a wet-compatible corneal sensor for recording ERG signal. Adapted with permission under a Creative Commons Attribution 4.0 International License from ref. 73. Copyright 2021 The Authors, published by Springer Nature. (g) Conceptual illustration of a bioadhesive adhering to human skin during heavy sweating and prolonged coverage. Reproduced with permission from ref. 102. Copyright 2023, John Wiley and Sons. (h) Schematic representation of microstructures generating reversible skin adhesion energy for patch applications. Reprinted (adapted) with permission from ref. 103. Copyright 2022, American Chemical Society.

devices under humid conditions, one can focus on surface compatibility, material selection, surface modification, and bio-inspired adhesives. Relying solely on intermolecular forces for adhesion between wearable electronic products and biological surfaces is ineffective. Therefore, it is essential to improve the capability of wearable electronic products to maintain excellent electrical performance in humid environments. Considering wet compatibility factors becomes critical to ensure that electronic devices adapt better to humid conditions. Additionally, the design of bio-adhesives and microstructures has proven effective in addressing the challenges of poor compatibility of wearable devices in humid environments. Wet adhesion designs for wearable devices can utilize materials compatible with wet surfaces, enabling the fabrication of wearable contact lenses. The human eye has a moist biological interface, and using commercial disposable soft contact lenses made of wet-adaptive materials can reduce eye damage and discomfort. Untreated commercial contact lenses possess unique properties such as biocompatibility, softness, breathability, transparency, wettability, and seamless adaptation to

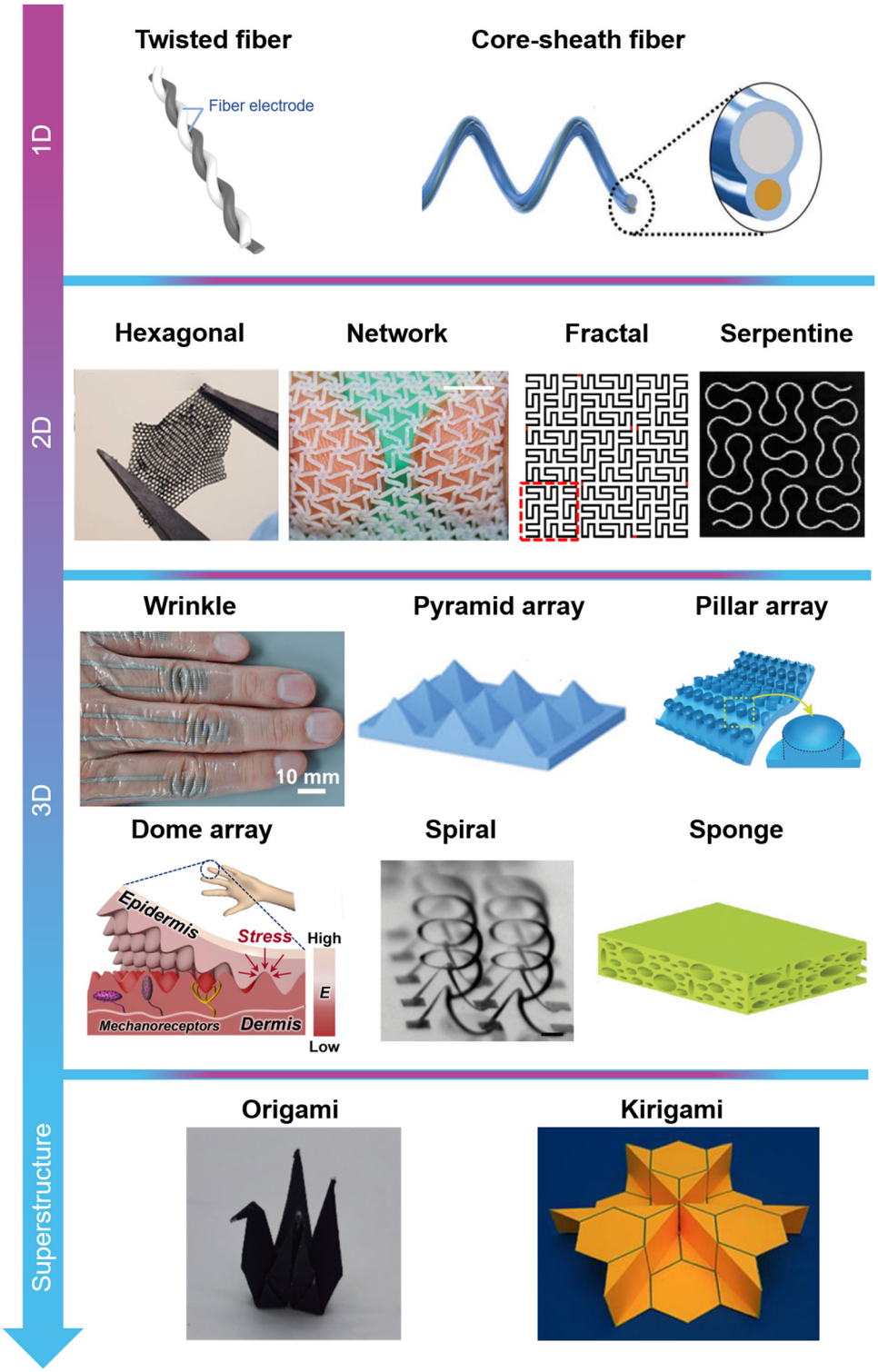

Fig. 3 Schematic diagrams of material structure design of wearable electronics. According to the different structures adapted to different external environments, they can be divided into four categories: 1D fibers, 2D sheets, 3D bionic structures and metamaterials. Image of a "Twisted fiber": reproduced with permission from ref. 105. Copyright 2024, Springer Nature. Image of a "Core–sheath fiber": reproduced with permission from ref. 104. Copyright 2020, John Wiley and Sons. Image of a "Hexagonal" structure: reprinted (adapted) with permission from ref. 109. Copyright 2020, American Chemical Society. Image of a "Network": reproduced with permission from ref. 111. Copyright 2018, Royal Society of Chemistry. Image of a "Fractal" structure: reproduced with permission from ref. 108. Copyright 2014, Springer Nature. Image of a "Serpentine" structure: reproduced with permission from ref. 108. Copyright 2014, Springer Nature. Image of a "Wrinkle" structure: reproduced under terms of the Creative Commons Attribution 4.0 International License from ref. 71. Copyright 2021 The Authors, published by American Association for the Advancement of Science. Image of a "Pyramid array": reproduced with permission from ref. 118. Copyright 2014, John Wiley and Sons. Image of a "Pillar array": adapted with permission under a Creative Commons CC BY License from ref. 116. Copyright 2018 The Authors, published by John Wiley and Sons. Image of a "Dome array": reprinted (adapted) with permission from ref. 120. Copyright 2018, American Chemical Society. Image of a "Spiral" structure: reproduced with permission from ref. 114. Copyright 2015, American Association for the Advancement of Science. Image of a "Sponge" structure: reproduced with permission from ref. 117. Copyright 2017, John Wiley and Sons. Image of an "Origami" structure: reprinted (adapted) with permission from ref. 115. Copyright 2024, American Chemical Society. Image of a "Kirigami" structure: reproduced with permission from ref. 122. Copyright 2017, Elsevier.

various corneal shapes. This corneal sensor is made by integrating serpentine circuits in a directly written form on these commercial contact lenses, maintaining direct contact with tears during human eye electroretinogram (ERG) tests (Fig. 2f).[73] By selecting appropriate bio-adhesives (polymers, hydrogels, and nanocomposites), adhesion performance can be maintained under humid conditions without affecting the functionality of wearable devices. Introducing bio-adhesives can provide adhesion in humid environments and waterproof effects. Polymer wet-adaptive electronic skin, made using electrospinning technology, adheres quickly to human skin and remains stable under humid conditions without adversely affecting skin health (Fig. 2g).[102] To mitigate the issue of skin damage, interface adhesion can be achieved through strong chemical interactions between the skin and adhesives. Many organisms in nature, such as tree frogs or mayfly larvae, have unique wet adhesion surfaces characterized by special micro/nano-structures or chemical compositions, allowing them to effectively attach to contact substrates and capture prey in complex environments. These biological wet adhesive surfaces have inspired the design of artificial analogues by mimicking their special micro/nano structures or chemical compositions. Inspired by bionic structures, a hierarchically arrayed octopus-inspired pattern has been designed to achieve interface adhesion by generating cohesive forces between liquid molecules, providing strong wet adhesion on the skin (Fig. 2h).[103] Additionally, constructing such micro/nano-structures by roughening the material surface or using hydrophilic or hydrophobic coatings can enhance the wet adhesion of wearable devices. For wearable devices, direct breathability and water resistance of the contact interface are particularly important in humid environments. Designing the material surface with hexagonal grid patterns to increase effective contact area and improve wet adhesion can achieve excellent wet adhesion effects.

2.2 Materials' structure

The successful manufacturing of wearable flexible electronic products relies heavily on the selection of materials. To achieve excellent conformal adhesion on rough, curved, soft, and textured biological surfaces and tissues, various types of materials need to be considered, including nanocomposites, hydrogels, and polymers. Additionally, besides material types, the material structure is also a crucial factor. By designing structures with one-dimensional (1D), two-dimensional (2D), three-dimensional (3D), and hybrid configurations, a skin-conforming surface matching the skin's texture can be achieved, meeting the adhesion, breathability, and stretchability requirements of flexible electronic devices. These structures include fiber structures,[104–106] patterned sheet structures,[107–113] biomimetic microstructures,[114–120] and superstructures (Fig. 3).[111,121–123] In fibers, the structure typically appears in a 1D form, primarily in the form of twisted fibers and core-sheath fibers, allowing effective adaptation to small strains. In the application of electronic tattoos, the substrate materials and circuit designs are generally presented in a 2D structure to facilitate conformal contact with the skin and deformation adaptation during movement. Common 2D material structures include four main types: hexagonal structures, network structures, serpentines, and fractal structures. Different types of structures serve different functions in various application scenarios. Hexagonal structures can mimic the internal structure of organisms to regulate the Poisson's ratio and adapt to the target strain range. Network structures can be appropriately matched based on the unique mechanics of biological tissues to adapt well to the stress–strain curve of human skin. Serpentine structures achieve good stretchability and conformity in limited area regions, while fractal structures disperse stress over specific areas, reducing stress concentration and increasing interface area to enhance adhesion, playing a particularly important role. Inspired by biological structures, mimicking these special biological structures in 3D form, such as pyramid structures, column arrays, dome structures, and porous sponge structures, effectively enhances the sensitivity of strain sensors and enhances adhesion to the interface. Additionally, common 3D microstructures in daily life, such as skin folds and spiral structures, have a ''folding'' effect, enabling materials to withstand greater tension when exceeding their deformation capacity. Therefore, they can be used to improve the ability of flexible electronic devices to maintain structural integrity during stretching. To reduce the occurrence of stress-induced cracking in materials under low strains, superstructures such as origami and kirigami have been developed, transforming flat material structures into three-dimensional surface features through specific processing. Origami structures achieve controllable deformation through different folding methods and angles, allowing flexible electronic devices to adapt to different shapes and surfaces. The structural design of kirigami can provide maximum area coverage, enhancing device stretchability through rotation and deformation, while ensuring mechanical integrity even under stress beyond the rated strain. Hence, it is essential to select suitable structures by evaluating application scenarios to meet the requirements of high area coverage, improved stretchability, and interface contact conformity in flexible electronics.

2.3 Wettability theory

The friction between traditional rigid inorganic materials and soft organic human tissues leads to various adverse consequences, including skin irritation, tissue damage, and a reduced signal-to-noise ratio (SNR).[124] Therefore, many researchers are actively working to advance and utilize more flexible and scalable structural designs, as well as the selection of materials, to address these issues. Flexible electronics are attached to the skin and can adapt their structure, texture, and shape to achieve various functions.[125–128] However, flexible electronics face challenges in the interaction occurring at the solid–liquid interface between flexible electronics and the skin. This hydrated environment arises from sweating during physical activity or exposure to external wet conditions such as rain or bathing. Hence, for the construction of flexible electronics, it is essential to consider the interactions between device surfaces with different wetting properties and liquids,

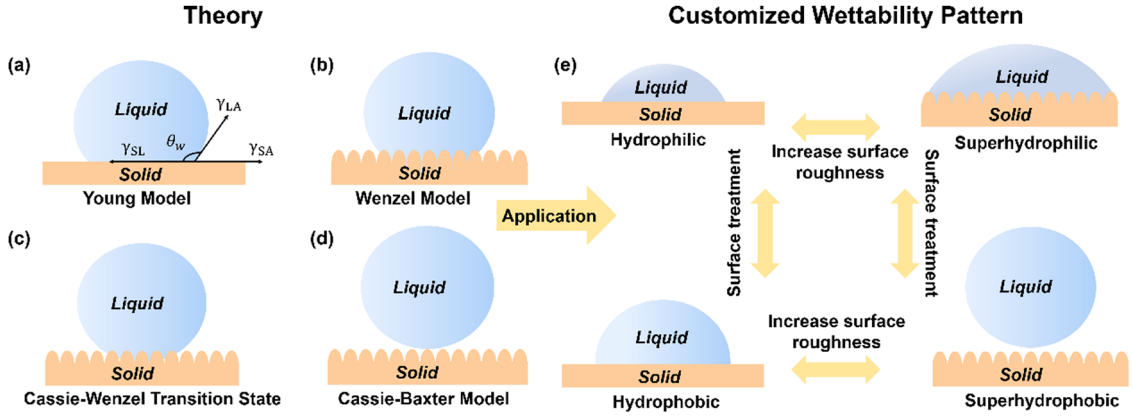

Fig. 4 Schematic illustration of wettability theory and construction of biomimetic structures. (a) Schematic of water contact angle (θ_w) in air. (b) Droplet on a structure's surface. (c) Droplet was detached from the structure's surface. (d) Droplet detached on a structure surface. (e) Controlling surface hydrophilicity and hydrophobicity transformation.

exhibiting distinct contact angles (CAs). Specifically, low (or high) surface energy results in CA values $>90^\circ$ (or $<90^\circ$), indicating a hydrophobic (or hydrophilic) state. To enable flexible electronics to adapt to environments with different wetting characteristics, the conversion between hydrophobic surface functional groups and hydrophilic functional groups must be controlled. Fundamentally, the control of the liquid wetting behavior on a solid surface is of utmost importance. The CA, which is the angle formed between a solid surface and the tangent drawn through the edge of the liquid droplet at the three-phase contact line, is a widely recognized parameter for measuring the wetting behavior of a liquid on a solid surface. According to the basic theory of wetting of a liquid on an ideally smooth surface proposed by Young in 1805, the CA can be measured using Young's equation (eqn (1)),[129] as illustrated in Fig. 4a:

$$\cos\theta_Y = \frac{\gamma_{SA} - \gamma_{SL}}{\gamma_{LA}} \quad (1)$$

where θ_Y represents the Young's CA of the liquid on a solid surface, and γ_{SA}, γ_{SL}, and γ_{LA} are respectively the solid–air, solid–liquid, liquid–air interfacial energies. When the CA of a liquid–solid combination is known, the equation can be calculated with high precision.

However, Young's equation is not sufficient for measuring the CA with credible precision for rough and structured surfaces or liquids that exceed the yield force. Two conditions may exist when wetting occurs on a rough or structured surface. The first condition is characterized by complete wetting of the surface with liquid, and the cavities of the rough structure are full of liquid. This condition is suitable for the Wenzel equation, as depicted in Fig. 4b. Using the Wenzel equation, the surface roughness was further considered to explain liquid wetting on a rough solid surface, as per the following equation:[130]

$$\cos\theta_w = r\cos\theta_Y \quad (2)$$

$$r = \text{roughness factor} = \frac{\text{actual surface area}}{\text{projected surface area}} \quad (3)$$

where θ_w represents the Wenzel CA on a rough solid surface, r indicates the roughness factor that is represented as the ratio of the actual surface area to the projected surface area, and θ_Y denotes the Young's CA on a smooth surface. The value of r is always greater than one. However, there is a defect in the Wenzel equation of continuous liquid wetting that does not explain liquid-wetting behavior with CAs greater than a certain degree, and discontinuous liquid wetting is observed, as seen in Fig. 4c. Thus, the Cassie–Baxter equation is used to interpret the presence of a porous external phase, *i.e*, an entrapped gas phase, on a solid surface with a prominent rough structure, which was the reason for the discontinuous contact between the beaded droplets and the solid surface, thereby reducing the contact between the beaded droplets and the protruding surface. The apparent Cassie–Baxter CA (θ_{CB}) takes into account the total contribution of each phase, which is referred to by the following equation:[131]

$$\cos\theta_{CB} = f_1\cos\theta_1 + f_2\cos\theta_2 \quad (4)$$

where f_1 represents the geometrical fractional contact area of a solid–liquid interface and f_2 represents the geometrical fractional contact area of a liquid–air interface. The solid–liquid and liquid–air contact fractions were summed to 1 as follows ($f_1 + f_2 = 1$). θ_1 indicates the CA of the liquid droplet on the solid phases. θ_2 denotes the CA of the liquid droplet on the air phases. The contact angle between the liquid and the air was 180°. If the solid fraction is expressed as f, the air fraction is expressed as $1 - f$. In summary, the Cassie–Baxter equation can be modified as follows in Fig. 4d:

$$\cos\theta_{CB} = f\cos\theta_1 + (1 - f)\cos 180^\circ \quad (5)$$

$$\cos\theta_{CB} = f\cos\theta_1 + f - 1 \quad (6)$$

Therefore, based on the above equation, surfaces with advancing and static water CAs greater than 150° were defined as superhydrophobic.[132] In contrast, surfaces with CAs less than 10° are defined as superhydrophilic.

2.3.1 Wettability method. Inspired by various natural plant microstructures such as lotus leaves, water lilies, and rose

petals, the construction of micro/nano-scale structures on substrate materials can be achieved to control wetting properties by mimicking the micro/nano-level structures of these plants.[133,134] Wetting properties primarily depend on the surface's micro/nano-structures and chemical composition.[135,136] Patterning of wetting surfaces can be accomplished by constructing different micro/nano-structures, while chemical surface modifications play a role in regulating hydrophilicity and hydrophobicity. Creating different micro/nano-structures helps to adjust the transition between substrate material's hydrophilicity and hydrophobicity, while chemical surface modifications can regulate the transition of substrate material's hydrophilicity to superhydrophilicity or hydrophobicity to superhydrophobicity (Fig. 4e). Treatment and wetting methods are summarized in Table 2.

2.3.2 Surface treatment. Each material possesses unique properties, resulting in differences in their wetting characteristics. When designing wetting properties for flexible electronics, selecting materials with appropriate wetting properties can prolong the device's lifespan and reduce interference from wetting environments on device signals. Therefore, commonly used surface treatment methods include chemical modification, plasma treatment, and UV irradiation. Chemical modification involves introducing chemical modifiers that react or interact with the material surface.[150] Specifically, chemical modifiers can form chemical bonds or functional groups with functional groups on the material surface, leading to changes in surface properties such as surface energy, hydrophilicity, or hydrophobicity. Thus, understanding the chemical composition of the materials used, such as functional groups, is beneficial for altering material surface wetting properties using chemical modification methods. Common hydrophobic functional groups include alkyl groups (such as methyl, ethyl, and propyl), fluorine-based groups, silicon-based groups, and nitro groups (Fig. 5a). For example, commonly used materials for encapsulation and substrates include silicone rubber (Ecoflex) and polydimethylsiloxane (PDMS). On the other hand, common hydrophilic functional group types include carboxyl, amino, hydroxyl, ethoxy, and siloxane groups (Fig. 5a). For instance, common thin-film substrate materials used for direct writing include polyethylene terephthalate (PET), polyimide (PI), and polyurethane (PU). Additionally, the type of material structure also aids in regulating wetting properties. Porous materials such as textiles, sponges, and nanonetwork structures can construct liquid drainage channels through surface treatment. This method typically controls the material's surface energy to adjust wetting performance. Higher surface energy leads to better spreading of liquids on the surface, resulting in stronger wetting. Generally, low surface energy reagents are substances with low polarity. Common types include fluorides such as polytetrafluoroethylene (PTFE), polyethylene, silicone oil, and Ecoflex, which have low surface energy, reducing interactions with other surface materials. Compounds containing fluorine atoms typically exhibit extremely low surface energy due to the high electronegativity of fluorine atoms, weakening their interactions with other molecules. In contrast to low surface energy reagents, high surface energy reagents typically exhibit high attraction and affinity on the liquid surface. Common types include hydroxides and oxides, such as glass surfaces, which usually have high surface energy because their surfaces readily interact with water and other polar solvents. Hydroxyl (–OH) compounds, amino ($–NH_2$) compounds, carboxyl (–COOH) compounds, and nitroso (–NO) compounds typically have higher surface energy as these compounds can interact with water molecules through hydrogen bonding. Thus, adjusting surface wetting properties can be achieved by controlling the free combination of functional groups in materials. The free combination of functional groups is achieved through intermolecular interactions such as van der Waals forces or electrostatic interactions. Besides utilizing the properties of functional groups for surface treatment, plasma treatment and UV irradiation are also commonly used surface treatment methods that can alter material surface properties, thereby affecting their wetting properties. Plasma treatment involves using excited gases to form plasma, generating high-energy ions, radicals, and excited-state molecules. These active species react with the material surface, causing physical and chemical changes to the surface. Plasma treatment can increase surface energy, making the surface more reactive, thereby enhancing wetting (Fig. 5b).[151] UV irradiation utilizes UV light with sufficient energy to break chemical bonds on the material surface, initiating a series of chemical reactions such as cross-linking, oxidation, or removal of surface contaminants. After UV irradiation treatment, the surface's active functional group content can increase, thereby improving wetting performance (Fig. 5c).[152]

2.3.3 Increasing surface roughness. Increasing surface roughness can enhance the contact area between the liquid and solid surface. When a liquid comes into contact with a rough surface, liquid molecules can enter into the tiny crevices and cracks, forming a larger liquid–solid contact area, which helps improve the wetting performance of surfaces with either hydrophilic or hydrophobic properties. Additionally, rough surfaces can also slow down the sliding of liquids on the surface, further enhancing the wetting performance. Therefore, constructing different or specific micro/nanostructures can significantly influence surface energy. These structures can control the surface morphology, texture, and topological structure, enabling surfaces to exhibit superhydrophobic or superhydrophilic properties.

Various methods, such as spraying, dipping, electrospinning, laser ablation, chemical etching, and electrochemical deposition, can be employed to prepare surfaces with different roughness levels. For instance, dipping involves immersing the substrate into a solution containing micro/nanoparticles or additives (Fig. 5d).[151] Similarly, spraying entails spraying a solution or suspension containing micro/nanoparticles or additives onto the target surface (Fig. 5e).[153] Both methods utilize the deposition or attachment of particles or additives onto the surface to alter its morphology and increase its roughness. However, these methods are not particularly suitable for treating porous materials because

Table 2 Treatment and wetting methods

Treatment	Method	Principle	Advantages	Limitations	Application fields	Ref.
Surface treatment	Chemical modification	Chemical modifiers react with or interact with the material's surface	Precise surface control, diverse options, and sustainability	Materials limitations, processing complexity, potential effects on durability and stability	Used for developing waterproof, paper-based flexible electronics	137
	Plasma treatment	Gas is heated to high temperatures, forming plasma and generating high-energy ions, free radicals, and excited molecules	Enhance surface activity, enable efficient surface modification, and suit all material types	Requires professional equipment, may affect material flexibility and mechanical properties, and demands strict control of processing conditions	Used to develop superhydrophobic smart clothing	138
	Ultraviolet irradiation	Photosensitive oxidation removes organic compounds material surfaces	Ideal for surface bond modification; The process is simple, low-cost, and efficient	May affect material stability; Requires specialized light sources and equipment; Limited by lighting coverage	Nanoribbon coatings are prepared for oil–water separation as a post-treatment	139
Increasing surface roughness	Electrochemical deposition	Metal ions in the electrolyte are reduced and deposited on the electrode *via* electric current	Simple, controllable, cost-effective; Enables high-resolution, high-purity deposition	Requires electrodes and electrolytes; Process depends on electrolyte composition	Used for patterning materials on flexible substrates	140
	Spray	A particle or additive solution is sprayed onto the surface for using spraying equipment	Simple, low cost, and suitable for large-scale application; Enables large areas coating	Controlling coating thickness is difficult; Solution and spray parameters need optimization	Textiles with motion sensing, self-powered interfaces, and superhydrophobicity	141
	Laser ablation	The laser locally heats the material surface, inducing thermal changes	High precision and resolution; Enables local, fine processing	Requires high-power lasers and control systems	For transparent and stretchable liquid metal electronics	142
	Dip coating	Immerse the surface in a particle or additive solution	Simple, low-cost, high-efficiency, and mechanized	Poor microstructure control and low precision	Used for developing breathable, hydrophobic wearable water droplet collectors	143
	Electrospinning	A high electric field ejects the polymer solution from the nozzle, forming fibers, and depositing a film on the receiver	Simple and cost-effective preparation	Affected by fiber formation conditions and electric field control	Used for developing environmentally friendly, high-performance waterproof breathable films	144
	Chemical etching	Material is exposed to a corrosive solution, causing chemical reactions with the surface	Low cost, high reliability, high capacity, and broad applicability	Surface topography is uncontrollable	Used to prepare microfluidic devices with controllable adhesion surfaces	145
	Soft lithography	Photosensitive materials are processed with soft molds	Enable high-resolution and high-purity structure preparation	Requires integration with other technologies	Used to develop wearable, self-cleaning hybrid energy harvesting systems	146
	Photoetching	A photoresist is applied to the photosensitive material, and light is projected through a mask. Exposure and development cause chemical or physical changes, creating the desired pattern	Achieve complex structures and patterns	Requires precision masks and lighting devices; Suitable only for photosensitive materials	Used to develop friction nanogenerators with superhydrophobic interfaces	147
	Laser direct writing	Laser beam focuses on the material surface to create fine structures, patterns, or textures	Precision machining and writing on the material surface	Equipment is costlyand the process range is limited	Used to develop wearable elastic skin with adjustable wettability	147
Customizing surface wetting pattern	Mask processing	Certain areas are exposed to the active medium to locally adjust the surface chemistry	Create intricate patterns in targeted areas	Processing range is limited, and pattern are prone to damage	Flexible sensors for biodegradable applications	148
	Printing	Prepare inks to meet specific wettability requirements	Low production costs and material savings	Improving print quality and achieving smooth printing is challenging	Used for designing and manufacturing flexible radio frequency identification antennas	149

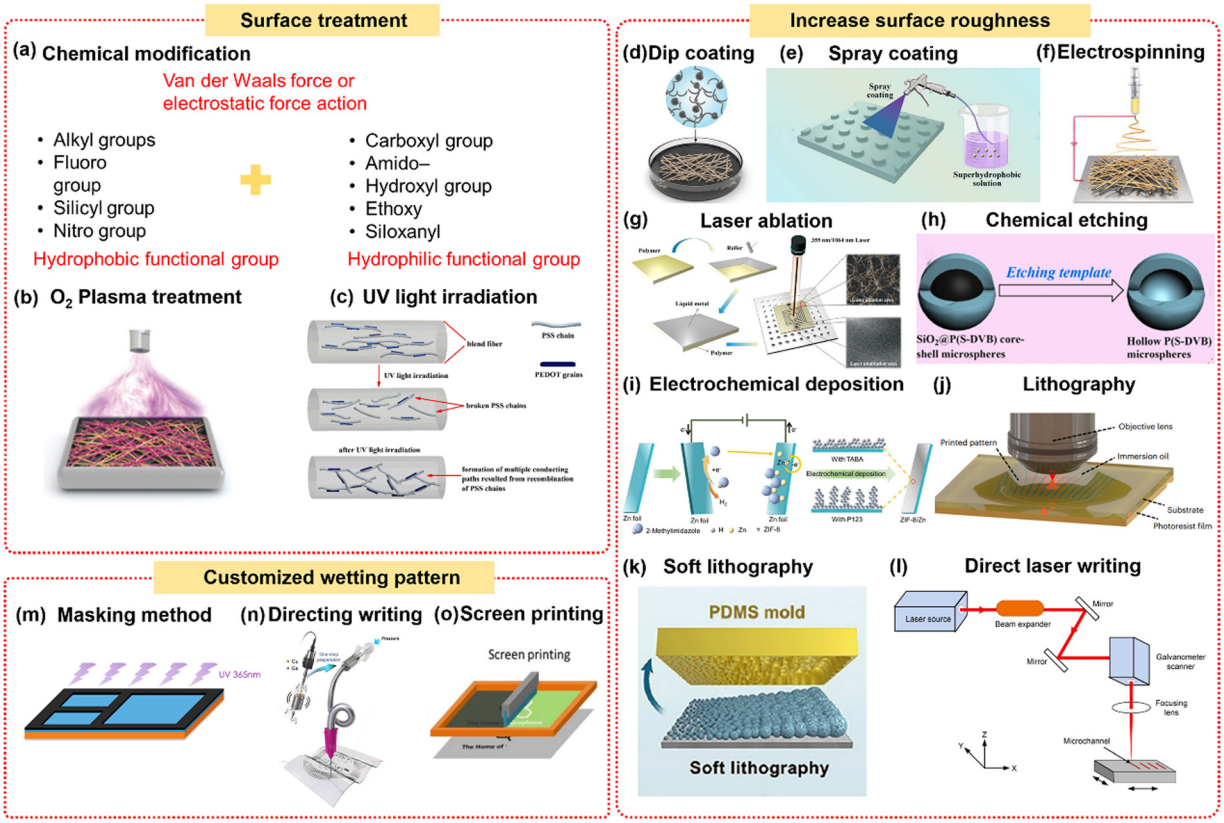

Fig. 5 Schematic illustration of wettability methods. (a) Common chemical modifications used in surface treatments. (b) Electronic textiles for unidirectional sweat transmission, electrophysiological monitoring and body temperature visualization. Reproduced with permission from ref. 151. Copyright 2023, John Wiley and Sons. (c) Molecular changes of poly(styrenesulfonate) chains when mixed fibers are illuminated. Reproduced with permission from ref. 152. Copyright 2020, Springer Nature. (d) Dip coating to apply the solution on the surface of the material. Reproduced with permission from ref. 151. Copyright 2023, John Wiley and Sons. (e) Schematic diagram of the preparation process of united superhydrophobic–hydrophilic polypropylene/graphene nanosheet films with mixed wettability, chemical resistance, and passive anti-icing properties. Reproduced with permission from ref. 153. Copyright 2022, Elsevier. (f) Electrospinning to prepare fiber fabrics with wettability. Reproduced with permission from ref. 151. Copyright 2023, John Wiley and Sons. (g) Schematic diagram of liquid metal circuit fabrication based on selective laser ablation. Reproduced with permission from ref. 154. Copyright 2022, Elsevier. (h) Preparation routes for hydrophilic and hydrophobic micro/nano dual-scale all-polymer particles. Reproduced with permission from ref. 155. Copyright 2022, Elsevier. (i) Schematic diagram of the ZIF-8/Zn electrode electrochemical deposition process. Reproduced with permission from ref. 156. Copyright 2022, John Wiley and Sons. (j) The process in which photoresist undergoes two-photon absorption, triggers chemical reactions and changes. Adapted with permission under a Creative Commons CC BY License from ref. 157. Copyright 2023 The Authors, published by Springer Nature. (k) Fabrication of hydrogels with surface roughness gradients by soft lithography. Reprinted (adapted) with permission from ref. 158. Copyright 2020, American Chemical Society. (l) Experimental device using a pulse overlap strategy to obtain straight microchannels. Reproduced with permission from ref. 159. Copyright 2023, Elsevier. (m) Manufacturing process of modified silk film with chemical patterning on the surface of silk film. Reprinted (adapted) with permission from ref. 160. Copyright 2019, American Chemical Society. (n) Schematic diagram of composite ink for direct writing printing. Reproduced under terms of the Creative Commons Attribution 4.0 International License from ref. 161. Copyright 2024 The Authors, published by American Association for the Advancement of Science. (o) Schematic diagram of a graphene ink screen printing process. Reprinted (adapted) with permission from ref. 162. Copyright 2019, American Chemical Society.

porous structures are susceptible to contamination by pollutants.

Electrospinning is a unique fabrication method that differs from spraying and dipping. It utilizes electrical forces under high electric fields to eject nano/microstructure solutions from a nozzle, forming fibers, which are then deposited onto a receiver to form a film (Fig. 5f).[151] This method is commonly used for the production of flexible electronic textiles and can be combined with other surface modification methods to construct higher roughness micro/nanostructures and achieve different wetting properties.

Laser ablation involves local heating of the material surface using a laser to induce thermal effects and create physical or chemical changes (Fig. 5g).[154] On the other hand chemical etching exposes the material to specific corrosive solutions. Active components in the solution react with the material surface, resulting in the dissolution of part of the material surface and the formation of tiny recesses or pores, thereby increasing surface roughness. By controlling parameters such as solution composition, temperature, immersion time, and stirring speed, the etching rate and surface morphology during the chemical etching process can be adjusted to regulate the material's surface roughness (Fig. 5h).[155]

Electrochemical deposition involves applying an electric current to the electrode surface to reduce and deposit metal

ions dissolved in the electrolyte solution onto the electrode surface, forming the desired metal deposition layer. This method can control the morphology, structure, and roughness of the deposition layer by adjusting parameters such as current density, solution composition, electrode material, and process parameters (Fig. 5i).[156]

In summary, the methods mentioned above for changing surface roughness lack precise control over surface roughness, which may result in uneven distribution of surface roughness. However, achieving changes in surface structure roughness in specific areas often requires expensive equipment and complex processes, such as photolithography, soft lithography, and laser writing technologies. Photolithography involves coating a photosensitive material on the substrate surface and then exposing it to light through a mask. Through exposure and development processes, the photosensitive material undergoes chemical or physical changes in the light-exposed areas, forming the desired pattern. Subsequently, the obtained pattern is transferred to the photosensitive material through etching, deposition, or other processing steps, thereby achieving the desired micro/nanostructure or pattern on the substrate surface (Fig. 5j).[157] Similarly, soft lithography involves applying a photosensitive material to the substrate surface, then gently pressing a flexible mold (typically made of PDMS) onto the photosensitive material surface, allowing the tiny structures on the mold to come into contact with the photosensitive material. Next, through light exposure, the light passes through the tiny structures of the mold, causing chemical or physical changes in the photosensitive material in the light-exposed areas. Finally, through subsequent processing steps such as development, the desired structure is transferred to the photosensitive material, thereby achieving the desired micro/nanostructure on the substrate surface (Fig. 5k).[158] Photolithography/soft lithography methods can control surface roughness, thereby changing the surface properties and functionalities of materials. Since photolithography/soft lithography techniques heavily rely on the role of templates in manufacturing micro/nanostructures, once the template is removed from the substrate surface, the constructed micro/nanostructures may be damaged, making this technology suitable for manufacturing relatively simple and regular surface structures. In contrast, laser writing has the advantage of precise processing and writing on the material surface. It creates fine structures, patterns, or textures on the material surface by focusing the laser beam on the material surface, adjusting the surface morphology and roughness (Fig. 5l).[159]

2.3.4 Customizing surface wetting patterns. When customizing surface wetting patterns, methods such as mask lithography, laser ablation, inkjet printing, and screen printing can be employed. During plasma treatment, the exposed surface areas through mask lithography undergo chemical reactions with active species in the plasma, introducing new functional groups or altering surface chemistry to adjust surface wetting properties. Similar to plasma treatment, during UV irradiation, molecules on the exposed surface areas through mask lithography absorb light energy, initiating photochemical reactions that lead to the formation or breaking of chemical bonds (Fig. 5m).[160] The areas protected by the mask in both methods prevent alterations to the surface. Laser ablation technology enables the customization of wetting patterns on the surface by adjusting laser energy and focusing. Inkjet printing technology utilizes inkjet heads to spray liquid ink onto the surface, forming the desired patterns (Fig. 5n).[161] Wetting patterns with specific chemical compositions and shapes can be created on the surface based on the wetting properties of the ink and substrate. Screen printing achieves rapid and efficient printing of desired patterns on the target surface with the assistance of designed patterns, ink, and suitable screens (Fig. 5o).[162]

3 Properties of wearable electronics

Wearable devices typically refer to electronic devices with properties such as flexibility and stretchability, usually manufactured on flexible substrates. From a materials perspective, the choice of materials is crucial for differentiating wearable devices from the traditional rigid ones. However, most flexible electronic devices with excellent electrical performance use substrate materials primarily composed of thin films (such as PET and polyvinyl alcohol (PVA)), gels (such as polyacrylamide gel (PAM) and polyethylene glycol (PEG) gel), and polymers (such as PDMS, PI, and PU). Therefore, the majority of substrate materials have poor breathability in humid environments, impeding the gas exchange between flexible electronic products and the surrounding environment, hindering moisture evaporation and heat control.[163] When wearable devices are worn for extended periods, the poor breathability of the substrate material and its strong adhesion to the interface can cause the device to adhere tightly to the interface, hindering gas exchange with the external environment. This can lead to poor breathability, affecting the evaporation of sweat and potentially causing sweat accumulation, which can result in skin allergies or dermatitis at the interface. Additionally, the accumulation of heat generated by the device during prolonged operation can pose a risk of burns to the wearer if effective heat dissipation is not achieved. Therefore, more effort is needed to address the challenge of poor breathability in substrate materials. Zhang *et al.*[164] proposed a Janus textile-embedded hollow microfluidic sweat sensor (Janus-t HMSS patch) platform to address the challenges of poor breathability and heat dissipation. The advantage of the HMSS patch is its minimal skin coverage area (approximately 0.22 cm^2), which promotes good breathability and sweat permeability when attached to the skin. This textile-structured wearable device ensures comfort and efficient heat dissipation during prolonged wear, avoiding skin inflammation, allergies, and reducing the risk of burns, providing a protective safety function. Wearable devices often need to conform and adhere closely to biological tissues (such as skin, muscles, blood vessels, brain, heart, and eyes, which are typically soft) to accurately capture and transmit physiological and biochemical signals, thus improving the accuracy and stability of monitoring data. However, biological tissues are

in different internal environments and typically have irregular surface textures. Therefore, wearable devices on these irregular and uneven tissue surfaces often struggle to conform to their curved profiles, leading to poor adhesion and conformity to tissue surfaces, reducing their adaptability and compatibility with biological tissues. The flexibility and stretchability of wearable devices ensure that they can adapt to various curves and dynamic movements of the human body, providing a comfortable wearing experience. However, most wearable devices require adhesion to biological tissue interfaces, but due to poor adhesion, they cannot achieve conformal adhesion to the interface. This can lead to asynchronous deformation and motion artifacts, reducing the accuracy of physiological signal monitoring and weakening signal transmission. Therefore, good adhesion and conformability of wearable devices are crucial for ensuring close contact with the skin, reducing device detachment caused by movement and effectively improving data collection accuracy and stability. Most adhesives made of silicone materials can attach to soft skin without causing rejection reactions by the biological body, showing great potential for application in providing biocompatibility. Therefore, adjusting the adhesion of adhesives when used as substrate materials for wearable devices can prevent damage to the skin surface while ensuring signal fidelity. Fu *et al.*[165] developed an elastic material capable of *in situ* adhesion on various surfaces. Adhesives made from this elastic material achieved ultra-high adhesion within 10 minutes, exceeding 3000 N m^{-1}. This strong adhesion is due to enhanced intermolecular forces between the adhesive elastic material and the adherent. Additionally, the adhesive can adjust intermolecular forces at low temperatures to reduce adhesion, making it easy to separate from the adherent. This method provides a meaningful approach to develop flexible electronic substrate materials with ultra-high adhesion on dry and wet surfaces for wearable devices. Besides the basic properties of wearable devices mentioned above, daily use inevitably encounters humid environments (such as rain, sweat, grease, *etc.*). Therefore, it is crucial to prevent moisture from entering the device and causing corrosive damage. Applying waterproof coatings to the device surface is essential. Surface treatments such as constructing gradient wettability surfaces or choosing materials suitable for wet environments can play an important role in adapting to wet conditions and extending the device's lifespan. As wearers demand wearable devices with multiple functions, such as health monitoring, wireless communication, and human–computer interaction, improving the comprehensive performance and user experience is necessary. The single function of wearable devices can no longer meet the needs of users. Wearable devices typically need to integrate various functions to meet users' diverse needs in healthcare, requiring improved design and functional integration, such as chip selection and data processing capabilities.

In conclusion, wearable devices can bend and stretch without damage or failure, making them suitable for various curved surfaces and irregularly shaped interfaces, such as smartwatches and health monitoring devices. These devices can better conform to human body curves, providing a more comfortable wearing experience. Compared to traditional rigid electronic devices, wearable devices are usually lighter because they can use thin plastic or polymer materials. In everyday use, wearable devices need certain waterproof and durability properties to ensure reliable long-term operation, considering environmental conditions such as water, sweat, and dust. Therefore, as summarized in Fig. 6, the future development of wearable devices should meet the following requirements such as good breathability, high stretchability, excellent waterproof performance, and controllable surface adhesion. Integrating these superior properties allows wearable devices to operate continuously and stably on moist surfaces while adhering to and conforming to soft skin interfaces, ensuring wearer comfort. This also promotes the development of wearable devices towards achieving more accurate biological signal monitoring and better user experience.

4 Types of monitoring signals in conformable electronics

Wearable flexible electronics can be employed for monitoring physiological,[148,149] biochemical,[163,164] physical,[166,167] and optoelectronic signals,[79,168] making essential contributions to the monitoring of individual health and the development of personalized medicine. To obtain a clearer and more intuitive understanding of the types of signals monitored by wearable electronics and their presentation forms, refer to Fig. 7.

4.1 Electrophysiological signals

Electrophysiological signals, arising from the electrical activities within a biological organism, play a crucial role in monitoring the functional status of cells or tissues for any potential abnormalities. In the era of continuous advancements in wearable electronic technology, portable monitoring of human electrophysiological signals has become possible, overcoming the constraints of size and cost associated with traditional devices. The application advantages of wearable electronics stem from their ability to adhere to the body's contours, making them suitable for monitoring conventional electrophysiological signals such as electrocardiogram (ECG), EMG, EEG, electrocorticogram (ECoG), and electrooculogram (EOG).

The generation of ECG is rooted in the role of electric currents in controlling heart movements, ensuring the circulation of blood throughout the body. ECG signals serve as a representation of cardiac electrophysiology. Recording these signals aids in assessing the rhythmicity and functionality of the heart, providing valuable information for diagnosing conditions such as arrhythmias and myocardial infarctions. This plays a proactive role in early diagnosis and the formulation of timely treatment plans for medical professionals.

When evaluating muscle activity and neuromuscular connectivity, recording and analyzing the electrical signals generated by muscle activity provide effective feedback regarding muscle function and neural conduction. This information

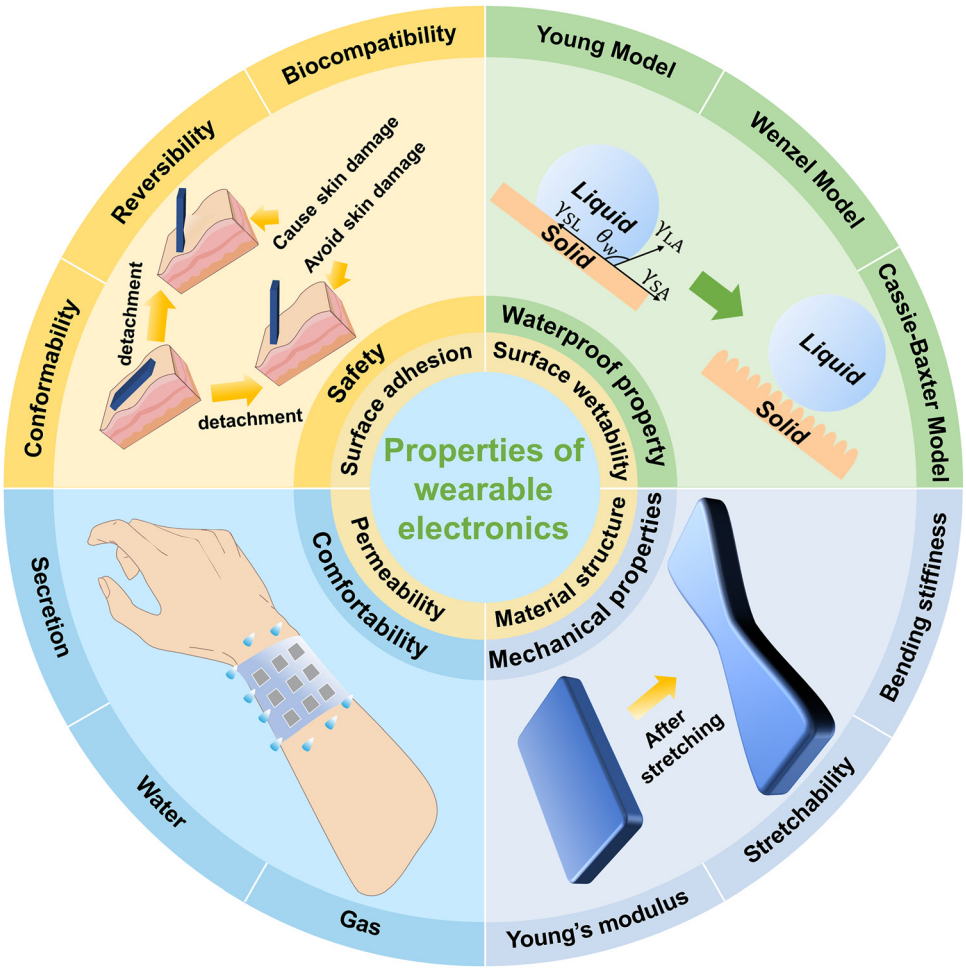

Fig. 6 Properties of wearable electronics.

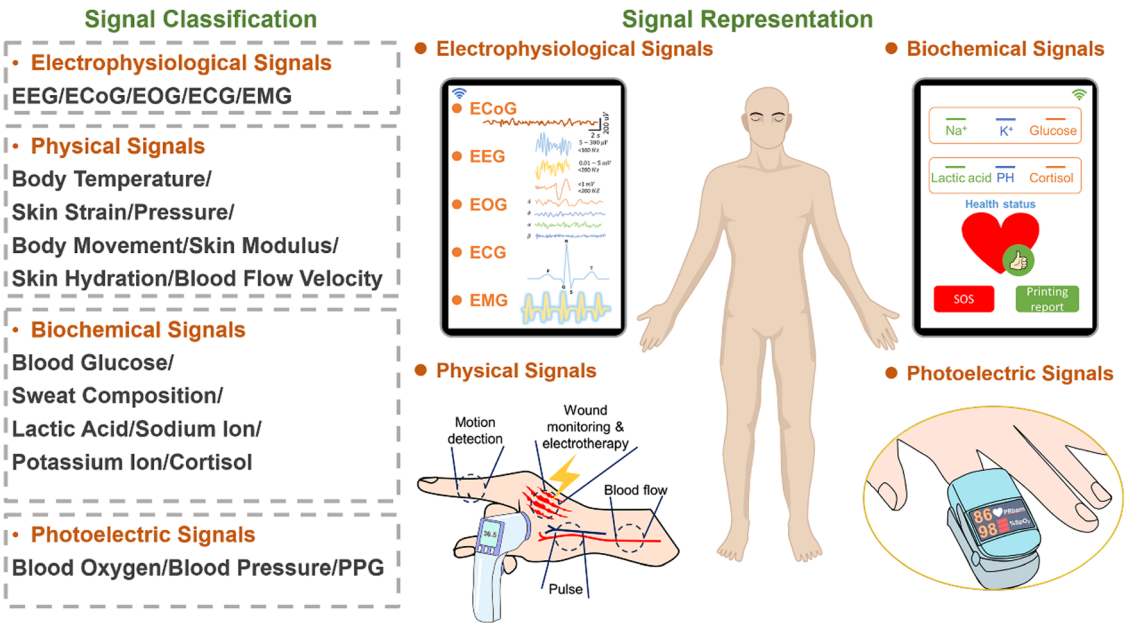

Fig. 7 Schematic classification of the different types of signals monitored using a wearable electronic device attached to the human body and the manifestations of different signals.

proves essential for diagnosing and monitoring various neuromuscular disorders, including myasthenia gravis, neuropathies, and peripheral nerve diseases.

Electrophysiological activity in the brain, observed through EEG and cortical brain signals, provides insights into whether any anomalies in brain function or state are present. Timely observations in EEG readings can aid in diagnosing epilepsy, studying sleep disorders, and addressing neurological diseases, providing a preventive and parallel means of treatment. ECoG represents the electrical activity of neurons in the brain, conveyed to the cortical surface through ion conduction. Analyzing these signals can be used to diagnose epilepsy.

Eye movements generate changes in electrostatic potentials, allowing for the diagnosis of retinal functional abnormalities through the monitoring of EOG.

In summary, wearable electronics facilitate the portable monitoring of various electrophysiological signals, offering a solution to the challenges posed by the size and cost of traditional equipment. Their ability to adhere to the body's contours makes wearable devices suitable for monitoring a range of physiological signals, including ECG, EMG, EEG, ECoG and EOG. This, in turn, enables early diagnosis, proactive medical interventions, and ongoing monitoring of individuals' health status.

4.2 Biochemical signals

Monitoring biochemical information enables the accurate assessment of physicochemical indicators at the deep molecular level in the human body. However, before the advent of wearable electronic devices, obtaining biochemical information required invasive methods, such as collecting blood samples for detecting various chemical components in the body. Blood sample collection, being an invasive method, involves pain, and repeated collection can cause discomfort and pose a risk of infection to patients.

With the continuous development of wearable electronics, wearable biochemical sensors transform the obtained human fluids (such as sweat, saliva, and tears) into electrical signals through specific reactions with detected biomarkers. This chemical-to-electrical conversion provides deep molecular information about the human body. As is well known, different types of bodily fluids can be obtained from various locations, distinguishing them from one another. Therefore, the diversity in obtaining bodily fluids is determined by the different types of fluids available. Sweat not only regulates body temperature but is also a crucial excretory pathway for maintaining normal body metabolism. Sweat contains abundant electrolytes and metabolites such as urea, uric acid, and lactate, as well as toxins. The concentrations of these substances in sweat are positively correlated with those in blood/urine, reflecting the individual's health status. The ongoing development of wearable biochemical sensors not only avoids damaging the human body invasively but also demonstrates the continued relevance of wearable electronics in humid environments. The coexistence of wearable electronics with sweat, a wet-compatible factor, does not compromise the ability to obtain biochemical information.

Tears in human eyes contain numerous biomarkers, including glucose, proteins, vitamin C, and pH, holding clinical significance for diagnosing the individual's health status. The correlation between glucose levels in tears and blood underscores its potential for assessing diabetic conditions. Tear proteins have been proven useful for early diagnosis of various diseases, including diabetic retinopathy, iridocorneal lesions, and dry eye syndrome. Tears also contain significant amounts of vitamin C, providing antioxidant protection, promoting wound healing, and treating corneal inflammation. However, collecting tears is challenging and requires stimulation (emotional, drug-induced, and electrical) to obtain them. Moreover, such stimulation increases hormone concentrations in tear secretion, rendering the results less convincing.

Saliva, obtained through chewing food, drinking, or oral ingestion of medications, includes various organic and inorganic biomarkers, such as glucose, nitrogen compounds, enzymes, antibodies, hormones, cytokines, and electrolytes. Compared to invasive blood collection methods, saliva collection is non-invasive and patient-friendly. In the era of the COVID-19 pandemic, collecting saliva for virus testing brings minimal discomfort and sufficient safety, allowing for rapid sampling and screening of infected individuals.

In summary, the development of wearable electronics has introduced wearable biochemical sensors that offer a non-invasive means of obtaining deep molecular information from the human body. The coexistence of wearable electronics with various bodily fluids, such as sweat, tears, and saliva, underscores their potential for continuous and comfortable monitoring of biochemical information. This not only enhances user experience but also provides valuable insights into human health.

4.3 Physical signals

Wearable electronic devices can adhere to the curved surfaces of the human body, enabling the monitoring of various biophysical signals, including strain at the body's joints, externally applied pressure, and body temperature. Body temperature is a crucial factor in maintaining normal physiological functions. Conformable electronics gather information by monitoring basic body temperature, local temperature around wounds, and skin temperature near superficial blood vessels, providing timely references for clinical diagnosis. Additionally, monitoring strain signals during human joint movements allows for the capture of subtle deformations. As blood flows within arteries, it generates different pressures, and blood pressure signals, such as pulse, can be monitored.

4.4 Photoelectronic signals

With the rapid development of wearable electronics, wearable optoelectronic biosensors utilize the absorption characteristics of oxygenated hemoglobin (HbO_2) and deoxygenated hemoglobin (Hb) to perform ratio optical measurements. The changes in the optical signals generated by this process allow real-time

monitoring of the percentage of blood oxygen saturation, providing essential support for assessing the health status of the human body. Flexible electronics are implanted into arteries to establish good contact for real-time monitoring of pressure changes in the arteries, ensuring a comprehensive safeguard for human health.

5 Applications of conformal and body-adaptive electronics

Surface modification is a key strategy to meet the diverse application requirements of wearable devices,[166,169,170] particularly in ensuring their stable adhesion to human skin under various environmental conditions, including dry and wet environments. Through the construction of meticulously designed micro/nano-structures, wearable devices can significantly enhance their wet adhesion and wettability, effectively addressing the challenges posed by moist environments such as rain and sweat.[166,170] Additionally, by leveraging the strengthening mechanisms of intermolecular forces and chemical bonds, the adhesion between the substrates or encapsulation materials of wearable devices and the skin interface can be markedly improved. Moreover, surface modification techniques utilizing hydrophilic or hydrophobic agents can precisely regulate the wettability of materials to meet the demands of different application scenarios.[167,171] As shown in Table 3, adopting appropriate manufacturing processes not only ensures close and stable contact between wearable devices and the skin interface but also flexibly adjusts their wettability characteristics, thereby greatly enhancing their adaptability and durability in wet environments. Compared to similar products without surface modification design, these meticulously designed wearable devices exhibit significant performance advantages.

5.1 *In vitro* conformal electronics

Wearable devices widely employ materials such as hydrogels, textiles, and various polymers like Ecoflex, PDMS, PET, PU, and PI. These materials are highly regarded for their exceptional softness, skin-friendliness, and biocompatibility. However, when interfacing with biological tissues such as skin and muscles, which have mechanical moduli ranging from 60 to 850 kPa and dynamically changing contact interfaces, the mismatch in mechanical properties and insufficient interface adhesion can lead to increased signal noise, reduced sensitivity to physiological signals, and even compromised device functionality. For materials with weak interface adhesion, traditional methods of securing devices with adhesive tapes often result in skin irritation or prolonged mechanical constraint, limiting the long-term application potential of flexible electronic devices. Flexible polymer materials, with their excellent stretchability, tear strength, and fatigue resistance, have become ideal choices for manufacturing wearable devices. They can withstand significant deformation without breaking and maintain stable performance under repeated deformations. To further enhance the conductivity and flexibility of wearable devices, researchers embed conductive nanomaterials (such as carbon nanotubes (CNTs), graphene, noble metal nanospheres, and nanowires) into stretchable elastomers, creating wearable devices that combine flexibility and conductivity. Among these, CNTs are the preferred reinforcing and conductive nanofillers for manufacturing stretchable elastomer strain sensors due to their unique high aspect ratio and superior mechanical, electrical, and thermal properties. Additionally, by finely processing thermoplastic materials, it is possible to create 2D films that can seamlessly conform to and adapt to the skin surface, significantly reducing irritation and damage while enhancing wearing comfort. This enables wearable devices not only to seamlessly adhere to the skin interface for monitoring physiological, biochemical, physical, and optoelectronic signals but also to be flexibly applied to areas such as hands, face, muscles, and joints on the body surface. These devices can accurately capture subtle signals related to human activity by utilizing the characteristic tension generated by joint movements. Therefore, careful selection of materials and meticulous design of structures are key to improving the interface adaptability of wearable devices. The adhesion and wettability between wearable devices and biological tissue interfaces become crucial factors in establishing reliable interface connections, enhancing device performance, and expanding application ranges.

To improve material adhesion to the skin surface, reducing material thickness can be effective. Xu *et al.*[167] used a cold pressing method to produce ultra-thin polyacrylamide (PAAm) and sodium alginate (PAAm–alginate) hydrogel films with thicknesses below 10 μm. These hydrogel films, with thicknesses ranging from 10 to 500 μm, showed Young's moduli between 34.3 ± 0.2 and 540.2 ± 81.3 kPa, comparable to human skin. When the thickness decreased from 500 μm (34.3 ± 0.2 kPa) to 10 μm (540.2 ± 81.3 kPa), Young's modulus increased tenfold. These hydrogel films can seamlessly adhere to and conform to the skin's texture. The expansion ratio of the hydrogel film, at a humidity of 90%, was 1.82 ± 0.02, demonstrating good water absorption and retention. Additionally, a high water vapor transmission rate (WVTR) of 1890.0 ± 134.4 g m^{-2} d^{-1}, three times that of thin PDMS, allows for effective management of skin moisture and sweat, ensuring a balanced microclimate between the device and the skin. These characteristics make them suitable for ultra-thin hydrogel interface optoelectronic devices. Hydrogel/electronic integrated patches can be repeatedly attached and detached without damaging the device or irritating the skin (Fig. 8a). Exploring skin breathability ensures that the design of wearable device materials meets skin breathability requirements, effectively addressing issues like itchiness and allergies caused by sweat accumulation at the skin interface. Using self-adhesive conductive polymers can improve adhesion without reducing device thickness. Zhou *et al.*[171] prepared a self-adhesive conductive polymer (SACP) by polymerizing a composite solution of poly(3,4-ethylenedioxythiophene)/poly(styrenesulfonate) (PEDOT/PSS) with a supramolecular solvent (β-cyclodextrin and citric acid). This polymer, with a low modulus (56.1–401.9 kPa), high elongation (700%), high interface adhesion (>1.2 MPa), and

Table 3 Innovative design of adhesive conformal electronics and wetting interfaces with a broad range of applications in the human body

Materials	Manufacturing methods	Interface designs	Sensing signal	Adhesion	Wettability	Advantage	Disadvantage	Application	Ref.
PAAm–alginate	Cold laminator	10 μm thick hydrogel film	Photoelectric signals	Long term skin adhesion over one week	N/A	High water-vapor permeability, extreme mechanical compliance, high optical transmittance, and biocompatibility field-effect transistors, organic electrochemical transistors, and organic photovoltaics	Adhesion force may not be precisely controllable	Organic	167
SACP	PEDOT:PSS composites with biocompatible supramolecular solvent	Strong interfacial adhesion *via* hydroxyl functional groups and charged molecules in SACP	EMG	High adhesion strength on diverse substrates (>150 N m^{-1} to PI, >120 N m^{-1} to PEEK, *etc.*)	N/A	Lower modulus (up to 56 kPa), low strain residual (<50% at 500% tensile strain), larger stretchability (up to 700%)	Under extreme environmental conditions such as high temperatures, low temperatures, and humidity, the performance of self-adhesive polymers may also be affected	Adhesive bioelectrodes for EMG monitoring	171
Au/polyethylene naphthalene (PEN) electrode	Mimicking the interfacial structure of microhairs	Pyramidal-shaped PDMS layer	JVPs	Excellent conformity and adhesion with pig skin *via* AR 10	N/A	Very small delay (<0.03 s) in a PDMS micropyramid and air-gap architecture	Under extreme bending or folding, Au/PEN electrodes may exhibit cracks or fractures, adversely affecting their conductivity and reliability	Monitor arterial tonometry or pulses in the neck	101
XSBR/SSCNT	Latex film-forming	Hydrogen bonding between hydrophilic sericin-modified CNTs and XSBR	Monitoring wrist movement	Skin-mountable heating device *via* XSBR/SSCNT sensor attachment to human skin	N/A	Low detection limit (1% strain), high stretchability (up to 217%), superior strength (12.58 MPa), high sensitivity (GF up to 25.98), high conductivity (0.071 S m^{-1}), lower percolation threshold (0.504 wt%)	Uneven dispersion of carbon nanotubes in elastomers leads to agglomeration, impacting the overall performance of the composite material	Electronic skins, personal health monitoring	172
LIG@PI/PDMS/PEIE	Utilizing LIG processing	Creation of conductive porous 3D LIG patterns through the carbonization of PI particles	ECG/EMG	Secure adhesion to curved surfaces without additional adhesives	Contact angle reduced from 51° to 6° with increasing PI content	Integrated multifunctional sensing platform for sweat biometrics: enhanced electrical and spatial modularity	Complex device operation and fine parameter control of laser direct writing technology increases production costs and process complexity	Real-time monitoring of ECG, EMG, and sweat glucose on the LIG@PI/PDMS/PEIE sensor platform	173
Biomedical adhesive (3M 1524)	Sweat-non-contact	Skin-interface platform featuring thermally-actuated, short straight fluidic	Monitor sweat information	Skin-interface platform adhered securely to the skin surface	N/A	Accurate chlorine, pH, and biomarker (creatinine, glucose) estimation	Deterioration of adhesive performance upon prolonged or frequent	Accurate and reproducible analysis of sweat rate, loss, and skin temperature	174

Table 3 (*continued*)

Materials	Manufacturing methods	Interface designs	Sensing signal	Adhesion	Wettability	Advantage	Disadvantage	Application	Ref.
		channels with a biomedical adhesive (3M 1524)					use, compromising device stability and reliability		
Polyurethane nananonet	Thermo-responsive gelatin hydrogel with nano-grid reinforcement for robust thin geometry	Ultra-thin interface design achieved by controlling hydrogel thickness below 10 μm	ECG	Self-adhesive skin interface for continuous 8-day high-quality electrophysiological monitoring	N/A	Robust (2.5 MPa, 696% elongation, 1000 cycles), skin-adhesive (176.8 μJ cm^{-2}), breathable (1669.3 g m^{-2} day^{-1}), anti-drying (12-day skin durability)	Complex nanotechnology and manufacturing processes elevate costs and difficulty	AI integration for precision diagnosis, treatment in digital health and precise control in human/brain–machine interfaces	175
AgNWs/parylene hybrid film material	Laser-cutting method for shape design	Kirigami-inspired 2D-to-3D geometric transformation	ECG	Conformal adhesion to finger and elbow joint skin for sensor attachment	N/A	Mechanically tunable 3D transformation enables operation on curved biological surfaces	Potential skin sensitivity to silver nanowires or interactions with other materials	Monitoring ECG signal	176
[2-(Methacryloyloxy) ethyl]dimethyl-(3-sulfopropyl) ammonium hydroxide monomer, crosslinker, photoinitiator, and ionic salt for composite hydrogel	Design of an integrated, standalone, and scalable device platform	Stretchable device platform with hydrogel electrodes, functional electronics, and coplanar serpentine copper network for signal processing, directly adherable to human skin	EMG	High mechanical compliance and robustness with skin-like Young's modulus (89.5 kPa), low hysteresis (<6.4%), and stretchability up to 30%, enabling comfortable integration on skin under various deformations	N/A	Accurate classification (>90%) of motion/speech features *via* combined data processed by a fully connected neuron-based 2D sequential feature extractor	Intricate formulation and synthesis requiring specialized equipment for precise ratio blending	Continuous, non-invasive monitoring of local vibrations and muscle activity of throat and other body parts, enabling activity differentiation *via* efficient convolutional neural networks and facilitating remote rehabilitation and disease diagnosis through cloud-processed data	177
cMaSK	Constructing the bionic structure of the gecko	Thin adhesion layer between f-PCB and m-PCB cases	Monitoring environmental and biological signals	Hook and loop mechanism for good adhesion with fabrics	N/A	High-accuracy face mask position classification (92.8% for males, 77.5% for females) using machine learning algorithms	Poor antibacterial performance	Monitor respiratory information and check the fit of mask wearing	69
Ultrathin PET film, CNT, MC	Hierarchical assembly approach	20 μm thin PET film substrate	BUW epidermal interface with an all-in-one function of sense	Conformal integration with the human body *via* a thin BUW epidermal interface	N/A	Rapid response time (<8 ms), high-precision touch detection	Poor breathability	BUW epidermal interface mounted on the palm for diverse HMIs	178
Polyurethane-acrylate-based polymer (s-PUA)	Mimicking the unique geometry of the suckers	OIAs	N/A	Increased adhesion forces under wet/oily conditions (37–154 kPa)	N/A	Adjustable adhesion force	Poor water resistance	Prevents sticky material fouling	179
OSCs	Electrospinning	Fluoroalkylated organosilane coating for omniphobic E-textile and OSCs	PPG	N/A	Repels liquids with low surface tensions (27.05 mN m^{-1})	Maintained breathability (air permeability >90 mm s^{-1})	Energy transmission efficiency can be affected by various factors, such as distance, obstacles, and the	Textile wristband-like battery-free photoplethysmography device	180

Table 3 (*continued*)

Materials	Manufacturing methods	Interface designs	Sensing signal	Adhesion	Wettability	Advantage	Disadvantage	Application	Ref.
							alignment between coils		
Janus silk E-textiles	Mimics the asymmetric structure of the lotus leaf	Hydrophobization *via* OTS dip-coating for silk textile	Biochemical signal	Unidirectional biofluid behavior reduces undesired wet adhesion ($\sim$0 mN cm^{-2}) for skin comfort	Hydrophilic silk fabric to hydrophobic–hydrophilic gradient *via* chemical bath and plasma treatment (WCA 0° to 139 $\pm$ 2.1° and back to 0°)	Silk-based yarn electrode integrated into hydrophilic Janus silk, multiple sweat target analysis	Washing and maintenance methods may be subject to certain restrictions	Wound dressing, disposable diaper, and breathing mask	181
Hydrophobic polyester (PE) and superhydrophilic nitrocellulose (NC)	Laser perforation	Janus PE/NC textile with asymmetric hydrophilic conical micropores for hydrophobic/superhydrophilic properties	N/A	High wet adhesion (21 $\pm$ 1 mN cm^{-2}) in wetted cotton textiles due to cellulose fiber hydrophilicity	PE layer-hydrophobic (80.0 $\pm$ 1.6°); NC layer-superhydrophilic ($\approx$ 0°) in air	Enhanced sweat transport and improved skin comfort (drier & warmer sensation) with Janus PE/NC textile featuring conical micropores	Production and processing costs are relatively high	Temperature regulation textiles	182
Surface nanostructures of the perfluorosilane-coated TiO_2 nanoparticles	Combination of superhydrophobic finishing and selective plasma treatment for gradient wettability porous spot channels in hydrophobic fabrics	Porous gradient wettability channels across hydrophobic fabrics	N/A	N/A	CA of 152°	High abrasion resistance (up to 10 000 cycles)	External environment that the coating comes into contact with can influence its durability and stability	Directional liquid transport fabrics/membranes	138
Transparent nanomaterials	Hybrid substrate with reinforced islands embedded in an elastic layer for strain distribution and protection	Planar mesh-like structures	Blood glucose	Smart contact lens fitted onto the rabbit eyeball	N/A	Superb reliability for mechanical deformations	Application is limited in scenarios requiring high resistance to external forces or deformation	Real-time sensing data access *via* smart contact lens	183
PDMS	Construction of pyramidal elastic microstructure	Interdigitated electrode design with pyramid elastic microstructures	Monitoring arterial pressure	Closer contact between the sensor and the polyolefin tube	N/A	Long-term durability and reproducibility	Poor breathability	Wireless pressure sensor for vascular health monitoring	60
Conductive PPEDOT NPs, PGA interpenetrated GelMA network	Nanoreinforcement effect of PPEDOT NPs in the PPG hydrogel	Well-connected electric pathway *via* evenly distributed PPEDOT NPs in a polymer network	ECG	Water absorption disrupts hydration layer for direct tissue-hydrogel adhesive group interaction	N/A	High flexibility and mechanical resilience for diastolic and systolic movements	The performance of the device is limited by the strength of the bonding between materials	Myocardial infarction therapy	184
Au/PI	Reduced layer thickness	Ultra-thin ECoG electrode design	ECoG	Enhanced flexibility for improved conformal contact	N/A	Enhanced conformal mapping area/sites and improved ECoG signal quality	Limited in applications requiring high degrees of bending or folding	Brain model testing with various animal device	185
Thin layer of hydrophobic PU nanofiber	Electrospinning hydrophobic PU nanofiber array onto a hydrophilic microfiber network	Self-pumping dressing	N/A	N/A	Water droplet maintains spherical shape (CA $\approx$ 146°) on a hydrophobic nanofiber array	Unidirectional drainage of excessive biofluid away from wounds	Poor wearing comfort	Self-pumping dressing for unidirectional biofluid drainage and wound protection	186

Fig. 8 Schematic diagrams illustrating the application of dry adhesion in flexible electronics. (a) Ultra-thin hydrogel films suitable for skin-integrated electronics. Adapted with permission under a Creative Commons CC BY License from ref. 167. Copyright 2022 The Authors, published by John Wiley and Sons. (b) Self-adhesive ink for monitoring EMG signal on the skin. Adapted with permission under a Creative Commons Attribution 4.0 International License from ref. 171. Copyright 2022 The Authors, published by Springer Nature. (c) Pressure sensors with microhair structures for highly conformal skin contact and pulse detection. Reproduced with permission from ref. 101. Copyright 2014, John Wiley and Sons. (d) Sensors mounted on the knees to monitor the corresponding signals of flexion, squatting, and jumping. Reproduced with permission from ref. 172. Copyright 2021, John Wiley and Sons. (e) The thickness of the device is reduced by means of laser induced graphene for monitoring ECG signal. Adapted with permission under a Creative Commons CC BY License from ref. 173. Copyright 2024 The Authors, published by John Wiley and Sons. (f) Build a skin interface platform with biomedical adhesives for monitoring biochemical information. Adapted with permission under a Creative Commons CC BY License from ref. 174. Copyright 2021 The Authors, published by Springer Nature. (g) ECG signal monitoring is realized by controlling material thickness by means of electrospinning. Reproduced under terms of the Creative Commons Attribution 4.0 International License from ref. 175. Copyright 2024 The Authors, published by American Association for the Advancement of Science. (h) Inspired by kirigami, a 2D flat surface is transformed into a 3D surface for monitoring EMG signal. Adapted with permission under a Creative Commons CC BY License from ref. 176. Copyright 2018 The Authors, published by John Wiley and Sons. (i) The ionic hydrogel interface was constructed to monitor physiological signals. Adapted with permission under a Creative Commons Attribution 4.0 International License from ref. 177. Copyright 2023 The Authors, published by Springer Nature. (j) Comfortable electronic devices attached to face mask for collecting environmental and biological data. Adapted with permission under a Creative Commons CC BY License from ref. 69. Copyright 2022 The Authors, published by Springer Nature. (k) HMI device is used to control the position movement of chess pieces. Adapted with permission under a Creative Commons CC BY License from ref. 178. Copyright 2023 The Authors, published by Springer Nature.

high conductivity (1–37 S cm^{-1}), is a promising candidate for soft electronic products. Adhesion tests proved that the self-adhesive film has strong bonding capabilities due to various interactions like hydrogen bonding, ionic interactions, and van der Waals forces. The citric acid and cyclodextrin components ensure good interfacial adhesion. The film demonstrated high adhesion performance on various substrates (PI > 150 N m^{-1}; poly(ether-ether-ketone) (PEEK) > 120 N m^{-1}; Al, Cu, PET >100 N m^{-1}; PTFE >80 N m^{-1}; PDMS > 30 N m^{-1}). Its conformal adhesion to human skin allowed it to be used as a

conductive interface between the skin and electromyogram, monitoring the biological electrical signals of the hand. SACP electrodes showed no significant signal attenuation even after ten uses (Fig. 8b). However, achieving real-time diagnostics remains challenging due to the irregular and fine topologies of the human body. Inspired by biological structures like insect leg gears, cricket cerci for airflow sensing, and beetle locking devices, Bao *et al.*[101] developed a flexible wearable pressure sensor with a micro-hair interface structure for effective contact with irregular skin surfaces. Using PDMS to create the desired geometric structure, the micro-hair interface enhanced non-invasive adhesion to the skin. This wearable device exhibited minimal delay (<0.03 s) and excellent stability over long-term cyclic testing (>3000 cycles under 10 kPa loading and unloading). The micro-hair structure improved signal strength when measuring weak signals like deep jugular vein pulses (JVPs) (Fig. 8c). Wearable devices can be adapted to and adhere to the skin interface by surface treatment and reducing device thickness. Strain sensors in wearable devices are crucial for detecting minor deformations caused by pulses and heartbeats and significant deformations from joint and muscle movements. Monitoring joint movements requires flexible materials with a wide sensing range and high sensitivity. Xu *et al.*[172] created carboxylic styrene butadiene rubber (XSBR)/hydrophilic sericin (SS) non-covalently modified carbon nanotubes (CNTs) sensors with good mechanical strength (12.58 MPa) and high conductivity (0.071 S m^{-1}) by incorporating SSCNTs into XSBR. These sensors, with CNTs evenly dispersed in XSBR, demonstrated the required flexibility and mechanical strength. They could stretch to 200% or even 400% of their original length without breaking, with a high gauge factor (GF) of 2.41 in a small strain range (0–3%), enabling the monitoring and identification of human activities. XSBR/SSCNT sensors exhibited good adhesion when attached to the elbow using 3 M VHB tape, monitoring large deformations during elbow movements (Fig. 8d). However, the uneven dispersion of carbon nanotubes in elastomers can lead to aggregation, affecting the overall performance of the composite materials and causing poor self-adhesion. To address this, Zhu *et al.*[173] proposed mixing PI powder with the PDMS precursor and PEIE additive (PEIE acts to form a complex with the Pt catalyst in PDMS to reduce its crosslink density, thereby enhancing adhesion). These mixed materials are cured at 80 °C for 3 hours, resulting in a stretchable bioadhesive composite material. By combining laser-induced graphene (LIG), PI particles are carbonized to form conductive porous 3D LIG patterns, while the original PDMS is converted into microstructured silica. This adhesive composite material (LIG@PI/PDMS/PEIE) has an extremely thin thickness of 100 μm, providing strong adhesion and low bending stiffness, allowing it to easily adhere to curved human skin or tissues without the need for additional adhesive layers. Additionally, by adjusting the content of PEIE, the adhesion strength of the PI/PDMS/PEIE composite material to the contact interface can be controlled. After more than 1000 cyclic tests, LIG@PI/PDMS/PEIE demonstrated stable electromechanical performance. Thus, the stretchability of LIG@PI/PDMS/PEIE can be further improved when combined with stretchable designs such as serpentine, wavy, or kirigami structures. This adhesive material can be used to create stretchable patches for capturing ECG signals with a SNR of 24.7 dB, comparable to the SNR of gel electrodes (26.4 dB). Due to its good adhesion strength, it can sustain adhesion for more than 24 hours. In reversible adhesion tests, after 1 and 2 cycles of peeling and reattaching, the patch still maintained high SNRs of 23.6 dB and 23.3 dB, respectively, during ECG measurements. More importantly, it can capture high-fidelity electrophysiological signals, such as ECG and EMG, even during dynamic deformation. The LIG@PI/PDMS/PEIE electrodes recorded electrophysiological signals during finger stretching or compression, showing no abnormal deviations in the sinus ECG waveform and maintaining a high SNR of 22.8 dB during a 15 s measurement (Fig. 8e). In terms of biochemical signal monitoring, Rogers *et al.*[174] proposed building a skin interface platform to accurately and reproducibly analyze sweat rate and loss, as well as skin temperature, using a soft wireless platform. This platform, constructed in a wearable form, integrates a thermal sensing module for sweat monitoring and bluetooth low energy functionality for wireless data transmission. The skin interface platform also includes a thermal actuator, short and straight liquid channels, and a biomedical adhesive (3M 1524) to measure upstream and downstream temperatures relative to the flow direction, capture sweat, and align with the channel pores and inlets to provide waterproofing and ensure the platform can adhere to the skin interface. Tests during cycling and rest for the sweat rate, sweat loss, and chloride, glucose, and pH levels in sweat revealed that at 10, 14, and 23 minutes of exercise, the sweat volume (Σf) reached 11.1, 20.7, and 31.63 μl, respectively. Chloride concentrations reached 61.7, 62.3, and 64.5 mM at 8, 14, and 26 minutes of exercise, respectively. Glucose concentrations were 39.2 μM and 70.6 μM at 14 and 23 minutes of exercise, respectively. These results indicate that the skin interface platform can better help understand the correlation between sweat-related parameters and the physiological state. Additionally, the skin interface platform demonstrated multifunctionality by measuring skin temperature, obtaining key parameters that complement sweat in the context of skin heat loss, body heat content, and central temperature regulation (Fig. 8f). To obtain long-term, high-quality electrophysiological signals, the key is to establish a stable, low-impedance interface between the electrode and human skin. However, the need for adhesives to achieve good adhesion effects makes it challenging to meet the requirements for long-term continuous health monitoring. Therefore, developing self-adhesive and breathable materials for long-term health monitoring is crucial. Wang *et al.*[175] proposed using gelatin as the hydrogel matrix and adding PU as the reinforcement layer prepared by electrospinning. The PU nanomesh is dip-coated in a diluted gelatin hydrogel solution at high temperatures (55 °C to 75 °C) and then gelled at physiological or ambient temperature, resulting in a 10 μm thick PU nanomesh reinforced breathable hydrogel sensor. This method reduces the thickness to 10 μm, significantly reducing bending stiffness and increasing skin

compliance. Due to its ultrathin geometry and porous structure, the ultrathin hydrogel exhibits a high WVTR of 1669.3 ± 23.5 g m^{-2} day^{-1}, almost the same as that of an open bottle hydrogel (1742.8 ± 18.3 g m^{-2} day^{-1}). Thus, the breathability of the ultrathin hydrogel is sufficient to allow gas diffusion from the underlying skin. Since the hydrogel contains a large amount of water, its resistance to drying is crucial. The ultrathin hydrogel contains glycerin, providing water-locking capability, with only a 1% water loss after 21 days of storage under ambient conditions. In contrast, the ultrathin hydrogel without glycerin dried rapidly within 24 hours, with a water loss of up to 41.1% after 2 days of storage. Cyclic stretching experiments showed that under 100% strain, the ultrathin hydrogel can withstand 1000 cycles of stretching and releasing, exhibiting excellent mechanical performance. Young's modulus of the ultrathin hydrogel is lower than that of human skin (0.1 to 2 MPa), making it highly compatible as a skin sensor. The ultrathin hydrogel enables ultra-irregular and seamless skin contact, with the peeled ultrathin hydrogel presenting a clear replication of micro-skin textures. Additionally, due to its ultralow Young's modulus and self-adhesiveness, the ultrathin hydrogel can move with the skin's natural motion during stretching and compression without the need for additional fixing devices or adhesives. After 200 adhesion/separation cycles, it still maintained good adhesion performance, with an area adhesion energy exceeding 90%, demonstrating the capability for repeated use in health monitoring. Therefore, this ultrathin hydrogel was used for long-term, continuous wireless ECG monitoring, successfully capturing characteristic waveforms with an SNR of 32.8 ± 1.6 dB, while commercial gels showed similar waveforms but a lower SNR of 29.7 ± 1.0 dB (Fig. 8g). Furthermore, ECG signal monitoring can also be achieved by introducing stretchability and/or deformability into planar electronic devices, allowing them to adhere consistently to 3D curved surfaces with minimal invasiveness. Hu *et al.*[176] proposed developing ultrathin silver nanowires (AgNWs)/parylene hybrid films and converting them from 2D to 3D geometries using kirigami-like laser cutting, for use in deformable structures on 3D surfaces. To develop ultrathin hybrid films, AgNWs were spin-coated on a silicon wafer to form an AgNW network. At room temperature, a parylene film was deposited on the silicon wafer *via* chemical vapor deposition to serve as a barrier layer protecting the AgNWs from oxidation in the environment. The hybrid film was then laser-cut into the target shape and the silicon wafer was peeled off as a single electrode sheet. The hybrid film was adhered to a PET substrate to achieve the 2D to 3D geometric conversion. Using the excellent conductivity and ultrathin conformal contact properties of the AgNWs/parylene hybrid film, the fabricated AgNWs/parylene hybrid film was used as the electrode for ECG signal monitoring. When attached to the skin, the impedance of the AgNWs/parylene hybrid electrode was 4.7 kΩ at 40 Hz, increasing to 15.6 kΩ after 20 cycles of attachment/detachment, still lower than 54 kΩ for commercial electrodes, demonstrating the stability of the AgNWs/parylene hybrid electrode in repeated attachment and detachment cycles during ECG signal monitoring (Fig. 8h). To improve the accuracy of monitoring signals, integrating machine learning is an effective way to mitigate motion artifacts generated during exercise. Gao *et al.*[177] proposed an independent stretchable device platform composed of hydrogel electrodes and functional electronic components, integrating a signal processing unit connected through a coplanar serpentine copper network. By doping AgNWs into an ionic hydrogel interface with a PDMS skeleton, they created an ionogel with stretchability and high conductivity, maintaining firm contact with the throat. This ionogel has a higher modulus (~200 kPa) providing greater load and strain-bearing capacity (tensile stress/strain of 14 kPa/200%). The added AgNWs not only provide high conductivity but also result in lower contact impedance compared to commercial gel electrodes, thus generating high-quality surface EMG signals. The composite hydrogel has lower tensile strain and about 8 times the peel force, enabling easy removal from the skin of infants or the elderly. Additionally, the composite hydrogel exhibits high mechanical compliance and robustness, including a skin-like Young's modulus of 89.5 kPa and low force hysteresis of less than 6.4%, with a tensile strain of 30%, ensuring comfortable integration on the skin during various deformations. The designed copper serpentine network has a maximum principal strain (3%) still lower than the fracture strain of copper (5%), facilitating high-quality monitoring during skin/body movements. This modified hydrogel, with excellent contact impedance, enables health monitoring (such as continuous, non-invasive monitoring of localized vibrations and muscle activity on the throat and other parts of the body) and, combined with an efficient convolutional neural network, can distinguish various activities, with data processing on a cloud server further promoting remote rehabilitation and disease diagnosis (Fig. 8i). While surface modification and reduced thickness enhance wearable device adhesion to the skin, hair and skin oils can still affect conformability and adhesion. Inspired by geckos, Dagdeviren *et al.*[69] developed a thin adhesive layer that improved the adhesion between various commercial masks and the skin, enhancing signal accuracy and sensitivity. Adhesion tests showed that the adhesive layer maintained repeatable adhesion with different masks, even after 100 cycles of attachment and detachment. A conformable multimodal sensory face mask (cMaSK) design, adapted to different face sizes and shapes, showed effectiveness despite facial hair (Fig. 8j). Human–machine interaction (HMI) electronic devices bridge the virtual world and humans, providing immersive interactive experiences. These devices need flexibility to conform to the skin surface, resisting bending deformation and ensuring continuous stable operation. Chen *et al.*[178] developed a bending-insensitive, unpixelated, and waterproof epidermal interface (BUW epidermal interface) for accurate HMI. This interface, comprising a 20 μm thick PET film, CNTs, and methylcellulose (MC), demonstrated excellent touch monitoring, adhesion, and durability. The thin PET film provided waterproofing, CNTs ensured interaction, and MC offered adhesion. The BUW epidermal interface exhibited fast response and recovery times (<8 ms) and maintained stability over

long-term cycling (>20 000 cycles). Its potential for wearable applications was evident from its conformal adhesion and signal transmission capability (Fig. 8k). The adhesion performance of wearable devices at the interface in a dry environment can be improved by adjusting the thickness of the device, adding fillers in the polymer, constructing micro/nanostructures, and constructing network crosslinking structures, so that wearable devices can exhibit conformal adhesion at the interface and improve the accuracy and reliability of monitoring signals. It provides a valuable idea for the preparation of wearable devices.

In dry environments, adhesives used to prepare wearable devices achieve interface adhesion through van der Waals forces, electrostatic forces, and hydrogen bonding interactions. However, under wet or underwater conditions, the effectiveness of these mechanisms significantly decreases, impacting interface adhesion. Therefore, developing an adhesive that works well under both dry and wet conditions is essential. Inspired by the biological structure of octopus suckers, Pang *et al.*[179] developed an adhesive with dome-shaped protrusions that can achieve reversible and repeatable adhesion on rough skin surfaces under various conditions (dry, wet, underwater, and oil-immersed). Under dry and wet conditions, the adhesive strength of the octopus-inspired architectures (OIAs) patch increased rapidly with preload. Moreover, comparing dense arrays of OIAs with different radii, it was found that a dense array of OIAs with a radius of 50 μm significantly increased normal adhesion under wet or oil-immersed conditions (approximately 37 kPa under wet conditions, 41 kPa under water, and 154 kPa in silicone oil). After more than 10 000 cycles of attachment and detachment, the OIA array remained highly adhesive and tensile-resistant. To verify its adhesion on rough skin, PDMS patches with OIAs loaded with phosphate-buffered saline (PBS) were compared to those without PBS. The patches with liquid PBS-loaded OIAs achieved high conformal attachment and detachment with a low preload of 10 kPa. Additionally, PBS-loaded OIA patches can be applied to wounds to promote healing (Fig. 9a). To ensure adhesion in wet and underwater environments while maintaining easy separation from the skin interface, Bartlett *et al.*[187] developed an adhesive inspired by octopus suckers' ability to independently control suction. This adhesive can activate or release adhesion. The adhesive elements mainly consist of flexible silicone arms covered with a soft pneumatic driving membrane. By adjusting the handle structure, the compliance of the suction cups achieves reliable adhesion in unstructured environments with low preload. The compliance adjustment rod can also independently control adhesion strength and toughness. Thus, octopus-inspired adhesive elements tightly bond with the skin interface, forming wearable gloves for autonomous adhesion control and dexterous underwater object manipulation. Adhesion is achieved by driving negative pressure to activate the adhesive when it contacts the acrylic substrate and reaches a predetermined load. The use of a soft elastomer material for the membrane and stem maintains reversible adhesion. This reversibility is achieved through active membrane control, enabling quick (<0.1 s) switching between high and low adhesion states, with adhesion strength switching 450 times from ON to OFF and remaining reusable over multiple cycles. The adhesion of wearable devices in wet environments (such as rain, sweat, grease, *etc.*) is usually disturbed by moisture, resulting in adhesion failure. The construction of micro/nanostructures is conducive to improving their adhesion at the interface in a wet environment, so that wearable devices can exhibit conformal adhesion at the interface and such adhesion can be self-adjusted, effectively guaranteeing the safety and comfort of wearers and providing a valuable way for the development of wearable devices.

The conformal and non-invasive bio-interface between wearable devices and human skin is highly beneficial for wearable electronic products. Therefore, it is advantageous to treat the material structures of the devices (such as designing them with bionic structures) and reduce the thickness of the devices to enhance adhesion at the device interface. In terms of material selection, self-adhesive polymers, for example, can improve interface adhesion. However, wearable devices inevitably encounter water environments when exposed to activities such as exercise, rain, or bathing. Accumulation of moisture at the wearable device interface can affect wearing comfort and performance. To maintain good performance in humid environments, the materials of wearable devices need suitable wettability. Common materials exhibit different wettability characteristics—textiles: cotton has high hydrophilicity, polyester shows low hydrophilicity, nylon has moderate hydrophilicity, and spandex has low hydrophilicity; polymer materials: Ecoflex is hydrophobic, PDMS is highly hydrophobic, PET is hydrophobic, PU is relatively hydrophilic, and PI is intermediate between hydrophilicity and hydrophobicity. For wearable devices that need to adhere to the skin for a long time, addressing moisture and heat management is essential. By designing the surface wettability of the wearable device, such as applying hydrophobic or hydrophilic coatings, changing the surface roughness through micro-nano structures, or modifying the chemical properties of the material surface *via* plasma treatment, wettability can be controlled. These methods help improve the material's breathability or transport sweat away from the skin, enhancing efficient gas exchange and moisture regulation, thus reducing the risk of inflammation and infection. Porous structures (sponges, textiles, nano-networks, serpentine curves, planar hexagons, *etc.*) are primarily used for breathability design. Huang *et al.*[188] developed sponge-structured fibrous cellulose aerogel flexible electrodes using thermal-induced phase separation. This unique sponge structure provides flexibility compatible with skin structure and porous properties for moisture absorption and evaporation. Additionally, coating with polypyrrole-wrapped silver nanowires (AgNWs@PPy) enhances antibacterial performance, reducing skin inflammation. While porous structures improve breathability, they also allow pollutant accumulation. Sweat from sweat glands during physical activity can penetrate these structures. Thus, surface treatment for waterproofing and self-cleaning is necessary. Martinez *et al.*[180] achieved hydrophobic

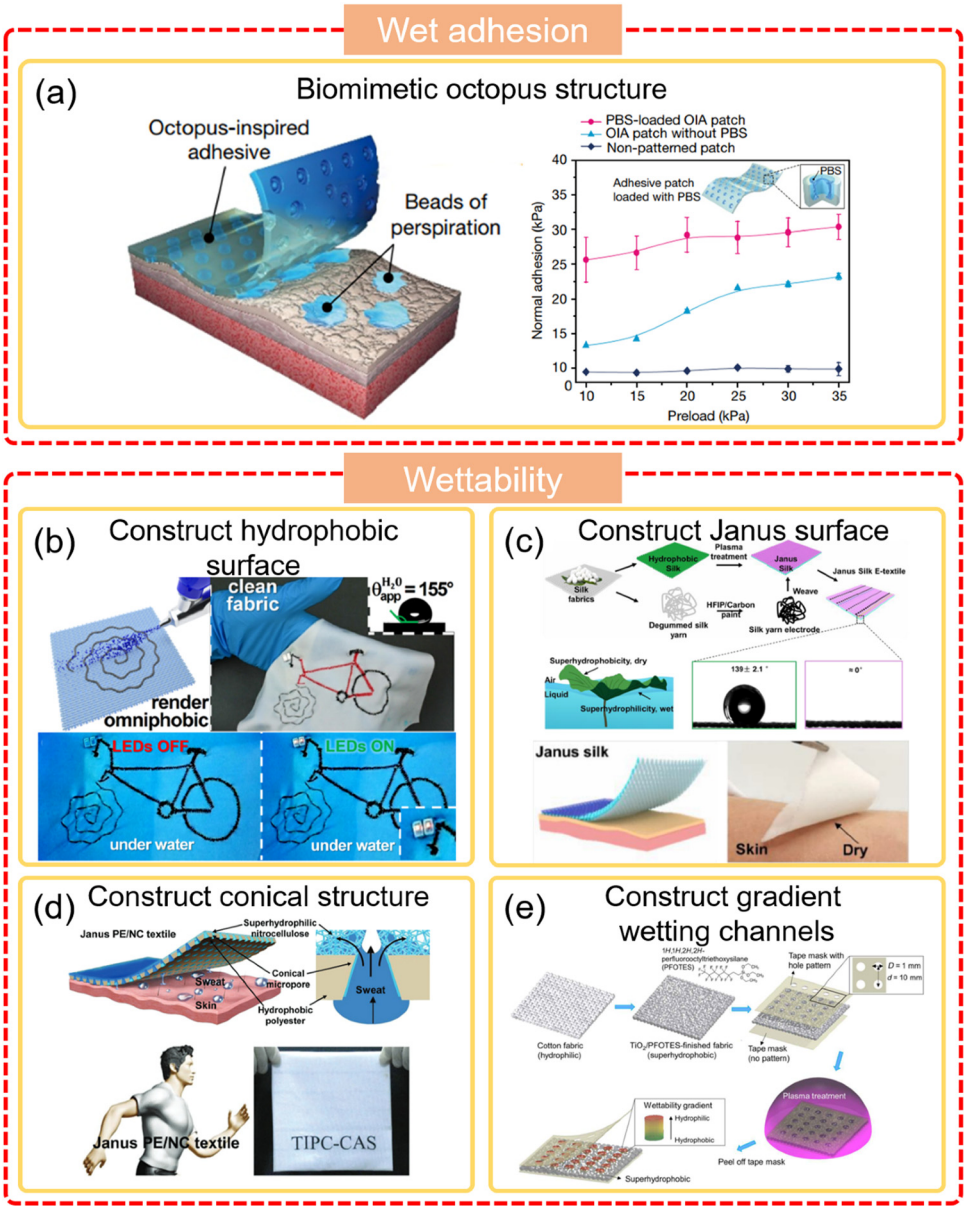

Fig. 9 Illustration depicting applications of wet adhesion in flexible electronics as well as methods for constructing wetting properties. (a) Adhesive with intricate, irregular topological structures adhering to moist, non-flat surfaces. Reproduced with permission from ref. 179. Copyright 2017, Springer Nature. (b) Wireless operation achievable when immersing hydrophobic electronic textiles based on OSCs in water. Reproduced with permission from ref. 180. Copyright 2021, Elsevier. (c) Janus silk electronic textiles utilized for unidirectional biofluid management and monitoring. Reprinted (adapted) with permission from ref. 181. Copyright 2021, American Chemical Society. (d) Biomimetic Janus textiles featuring conical micro-pores directing sweat output pathways on the human body. Reproduced with permission from ref. 182. Copyright 2019, John Wiley and Sons. (e) Formation of gradient wetting point channels across fabric thickness, endowing skin-like textiles with dual properties of directional water transport and hydrophobicity. Reproduced under terms of the Creative Commons Attribution 4.0 International License from ref. 138. Copyright 2020 The Authors, published by American Association for the Advancement of Science.

and oleophobic properties by spraying a fluorinated alkyl silane solution onto all-polymer-based coils, repelling low-surface-tension liquids (water, sweat, blood, and most oils). This behavior results from the interaction between fluorinated polymer particles and the surface, with particle sizes below 10 μm aiding in covalent attachment without interfering with textile gas transmission (breathability 90.5 mm s^{-1}). Additionally, omniphobic silk-based coils (OSCs) demonstrate excellent strain tolerance up to 500% and rapid response and recovery (30 ms). Their serpentine pattern design makes OSC-powered electronic textiles flexible, twistable, and highly stretchable (strain up to ε = 100%), not restricting movement or comfort. OSC-powered textiles' omniphobic properties allow operation even when fully immersed in water, protecting embedded electronics from short circuits, sweat, washing cycles, or accidental spills. They maintain performance after over 100 wash

cycles, including soaking and drying, with a static CA of $\theta_{app}^{H_2O} = 155°$. Integrating OSCs into textiles *via* sewing enables continuous wireless power supply through magnetic resonance coupling. For example, OSC-sewn wristbands can power photoplethysmography (PPG) sensors, wirelessly transmitting real-time PPG signals to paired devices for non-invasive heart health monitoring (Fig. 9b). Constructing anisotropic surface geometries with roughness and wettability is an effective strategy for unidirectional fluid transport, reducing unnecessary moisture and sticky experiences and showing great potential for accelerating sweat evaporation and body temperature regulation. Designing and modifying silk materials can provide ideas for comfortable electronic textiles in humid environments. Zhang *et al.*[181] developed Janus dual-sided electronic sportswear inspired by lotus leaf asymmetry. One side is hydrophilic silk fabric (with a water contact angle (WCA) of 0°), and the other side is hydrophobic (WCA of 139 ± 2.1°) achieved through octadecyltrichlorosilane (OTS) solution treatment and plasma processing. This Janus wettability structure effectively transports sweat unidirectionally, keeping the hydrophobic side dry and the hydrophilic side moist, regulating skin humidity. Traditional textiles (silk, cotton, polyester (PE), and wool) exhibit different adhesion levels at the skin interface, ranging from 14.6 to 18.5 mN cm^{-2}. Silk garments exhibit negligible skin adhesion (as low as 0 mN cm^{-2}). These data indicate that the silk scaffold forms a dry interface with the skin, eliminating adverse wet stickiness. Silk electrodes, created by adding conductive carbon paint to hexafluoroisopropanol-stabilized degummed silk yarns, are selectively woven into the Janus silk substrate's hydrophilic side as biofluid sensing electrodes. These are connected to a printed circuit board to record discrete changes in sweat, glucose, pH, and K^+ every minute. Collected data are transmitted wirelessly to smartphones for signal transduction, conditioning, processing, and analysis. The synergy between the Janus silk substrate and silk electrodes removes excess biofluid unidirectionally, creating a comfortable microclimate and enhancing skin comfort. During exercise (0–10 min), the temperature of the silk-covered area is slightly lower than the original silk area (*e.g.*, a 1.5 °C decrease at 10 min) due to accelerated sweat evaporation and heat removal. Janus silk has a shorter response time for recording biofluid content during exercise than original silk, improving sampling and analysis efficiency (Fig. 9c). Textile moisture transport performance significantly affects physiological comfort, largely depending on surface wettability. Traditional hydrophilic textiles like cotton become saturated with sweat, causing unwanted wet stickiness, while hydrophobic textiles like PE repel water externally but not internally. Hence, developing new functional textiles for efficient sweat transport and preventing overcooling is crucial. Inspired by biological structures like cactus spines and spider silk, which have unique asymmetrical gradient structures for directed water transport, constructing asymmetric surface structures enhances rapid sweat removal. Wang *et al.*[182] constructed asymmetric hydrophilic conical micropores on commercial Janus PE/nitrocellulose (NC) membranes through laser ablation and modification. Contact angle tests showed that the PE layer exhibited significant hydrophobicity in air (80.0 ± 1.6°), while the NC layer exhibited significant superhydrophilicity (≈0°). Embedding this structure into textiles resulted in Janus PE/NC textiles with hydrophobic/superhydrophilic interface effects. The hydrophobic layer maintained a relative water content close to zero, whereas the superhydrophilic layer's relative water content increased rapidly (1246% within 35 s). This demonstrated that once water was brought into contact with the hydrophobic layer, capillary forces and enhanced conical micropores quickly transported water through the Janus PE/NC textiles to the superhydrophilic layer. This confirmed that Janus PE/NC textiles could unidirectionally transport liquid from the hydrophobic to the superhydrophilic layer. Observing the dynamic transmission process of methylene blue-dyed aqueous solution on the hydrophobic layer of Janus PE/NC textiles further validated this. After absorbing water, Janus PE/NC textiles exhibited very low skin adhesion (0 mN cm^{-2}). This is because the wet skin covered by Janus PE/NC textiles dried within seconds due to spontaneous directional water transport, resulting in minimal adhesion to human skin. In contrast, wet cotton fabrics typically exhibited high wet adhesion (21 ± 1 mN cm^{-2}) due to the hydrophilic nature of cotton cellulose fibers. Thus, Janus PE/NC textiles can reduce unwanted wet adhesion (Fig. 9d). Designing wearable devices with wettability or hydrophilic treatment, or using multilayer materials with different wettability as asymmetric structures, is crucial for developing wearable devices with both wettability and conformal adhesion. Wearable devices developed using these methods show that liquids tend to transfer from the hydrophobic (*e.g.*, hydrophobic or oleophobic) side to the hydrophilic (*e.g.*, hydrophilic or oleophilic) side before the hydrophilic side saturates. However, they face challenges in transporting liquids in the opposite direction. To overcome this, Lao *et al.*[138] were inspired by the skin's ability to autonomously expel sweat to protect the body from external liquid pollutants. They developed a fabric with directional liquid transport similar to "skin". Hydrophobic treatment was applied to hydrophilic cotton fabric by adding TiO_2 nanoparticles coated with 1*H*,1*H*,2*H*,2*H*-perfluorooctyltriethoxysilane (PFOTES) to create a superhydrophobic interface. CA tests showed the superhydrophobic fabric had a CA of 152°, compared to 0° for the original cotton fabric. Using a mask method, selective plasma treatment created patterned areas on the fabric, resulting in porous gradient wettability channels. Plasma treatment produced significant CA differences between exposed spots and non-exposed non-spot areas. The non-exposed areas' CA decreased slightly after plasma treatment, while the exposed spots' CA significantly decreased, forming a wettability gradient through the fabric's thickness. When used for unidirectional liquid flow, the fabric's primary superhydrophobicity repelled transported or external liquids from the surface. To demonstrate directional water transport, a blue silica gel bead-filled glass container was covered with the fabric and observed for color change, indicating moisture entry. Superhydrophobic finishing and plasma treatment did not adversely affect the

WVTR and air permeability at 35 °C, but they increased tensile strength and modulus due to nanoparticle incorporation. After wear cycles, the CA of non-spot areas slightly decreased, such as to 139° after 10 000 cycles ($P > 0.05$), and further to 116° after 25 000 cycles ($P < 0.05$). This method's advantages support developing smart high-performance clothing, especially sportswear, with significant value for industry and consumers (Fig. 9e). When wearable devices encounter a wet environment on the human body, their waterproof performance can be effectively improved by designing the wettability of the material surface, such as constructing a hydrophobic coating. Constructing Janus asymmetric structures enables the device to transport sweat and enhances its self-cleaning capability. Building gradient wettability structures facilitates sweat transport, helping to maintain a dry interface. These wettability design strategies offer new approaches for developing the waterproof and self-cleaning functions of wearable devices.

5.2 *In vivo* conformal electronics

In exploring innovative designs for the interfaces between wearable devices and human tissues, the diversity and unique environmental characteristics of organs such as the eyes, heart, brain, and blood vessels (especially their softness and moist environments) have become core elements in the design process. To achieve long-term, stable interactions with low damage to biological tissues, particularly when in contact with soft tissues like the brain, modulus matching becomes a key design factor. Traditional neural probes, which use high-modulus materials such as metals or silicon (with moduli reaching hundreds of GPa), exhibit significant mechanical mismatches with brain tissue, often inducing inflammatory responses and chronic neural damage. The advent of stretchable electronic devices actively addresses this technical challenge, ushering in a new era of high adaptability to complex biological surfaces and dynamic environments. These advanced wearable devices, with their exceptional flexibility and adaptability, can closely conform to various complex human surfaces, such as the cerebral cortex, ensuring ultimate comfort and stability in wear. To further enhance the performance of devices in moist environments, innovative material selection strategies (such as incorporating moisture-compatible materials) and sophisticated structural designs (such as constructing micro/nano-structures and optimizing device thickness) are employed to achieve fine control over the wettability of biological tissues. Optimizing wettability not only helps to enhance interface harmony but also effectively reduces interface friction, lowering the risk of potential inflammatory responses, thereby ensuring the continuous stability and accuracy of monitoring signals while improving the overall comfort and safety for the wearer. Moreover, by carefully adjusting the adhesion between wearable devices and the interface (using advanced methods such as micro/nano-structures and adding specific fillers into polymers), the devices can be more securely attached to tissue surfaces, significantly reducing issues of signal fluctuation caused by displacement or detachment. Special treatments of the material surface not only endow the materials with excellent mechanical properties, effectively mitigating potential damage caused by mechanical stress mismatches to the tissue, but also significantly enhance their biocompatibility, reducing the risk of immune responses during implantation or wear. Coupled with stretchable and diversified structural designs, these devices can flexibly respond to the dynamic changes of the biological body, optimizing interface interaction experience and further improving the efficiency and accuracy of signal transmission. Therefore, actively exploring new materials with high modulus matching to biological tissues and innovative structural designs has become the core task in regulating the wettability and adhesion of wearable device interfaces. This is also key to promoting the in-depth application of wearable technology in fields such as medical care and health monitoring.

Park *et al.*[183] introduced a revolutionary soft smart contact lens. This contact lens achieved breakthroughs in materials science by using selected silicone elastomer materials, ensuring excellent wettability and comfort, mimicking the natural moisture environment of the eye, and effectively reducing discomfort from prolonged wear. Additionally, advanced interface adhesion technology allows the contact lens to maintain stable monitoring during eye movement or blinking, providing users with seamless health monitoring experiences. The core technological highlight of this contact lens is the integration of a continuous network made of 1D ultra-long silver nanofibers. This innovative design not only endows the contact lens with stretchable and transparent electrode properties but also equips it with antenna functions, demonstrating excellent mechanical durability and efficient signal transmission on curved structures. Placing this design outside the pupil avoids visual interference while ensuring the sensor operates continuously and stably. To further enhance the device's durability and its ability to adapt to eye movements, a stress-adjustable hybrid structure of the substrate was introduced, comprising mechanically reinforced islands and elastic joints, effectively resisting mechanical deformation caused by eye movements and protecting the delicate internal electronic components from damage. Moreover, by integrating advanced wireless communication technology, this contact lens can transmit collected biological data (such as glucose, cholesterol levels, and electrolyte concentrations) to smartphones or other smart devices in real-time, providing users with immediate and accurate health monitoring feedback (Fig. 10a). Further advancements have been made in applying wearable devices to arterial health monitoring. Bao *et al.*[60] proposed using biocompatible PDMS as the packaging or encapsulating material, adjusting the PDMS ratio (23 : 1) to achieve low compressive modulus properties for manufacturing pressure-sensitive elements. Copper, due to its exceptional electrical conductivity, is widely utilized in electrodes, electrical interconnects, wireless antennas, and other applications. In the construction of wireless capacitive sensors, to ensure human safety, PDMS is commonly employed as an encapsulation material to effectively encapsulate the copper layer, thereby offering a protective function. These wireless capacitive sensors can be wrapped around arteries

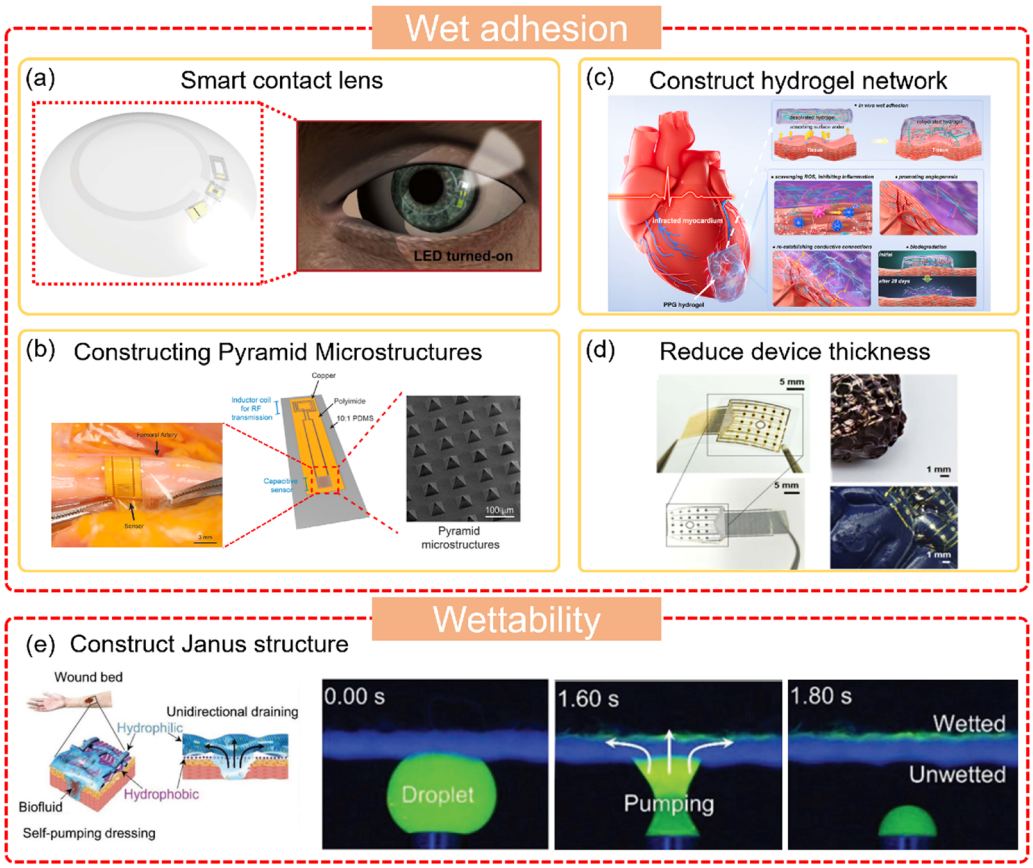

Fig. 10 Schematic diagrams illustrating the applications of wet adhesion and wettability in the human body. (a) Stretchable transparent smart contact lens system. Reproduced under terms of the Creative Commons Attribution 4.0 International License from ref. 183. Copyright 2018 The Authors, published by American Association for the Advancement of Science. (b) Biocompatible flexible arterial pressure sensor. Adapted with permission under a Creative Commons CC BY License from ref. 60. Copyright 2021 The Authors, published by Elsevier. (c) Hydrogel self-adhesive cardiac patch for treating myocardial infarction, composed of conductive polydopamine hybridized PPEDOT NPs and a PGA interpenetrating GelMA network. Reproduced with permission from ref. 184. Copyright 2024, Elsevier. (d) Ultra-thin brain electrode array for conformal contact. Reproduced with permission from ref. 185. Copyright 2020, IEEE. (e) Asymmetric structure self-pumping dressing for wound healing. Reproduced with permission from ref. 186. Copyright 2018, John Wiley and Sons.

during surgery, continuously monitoring post-operative arterial health, including potential complications such as stenosis, reduced blood flow, and thrombosis. To improve sensor sensitivity, the material structure was designed into pyramid-shaped elastic microstructures, enhancing adhesion between the device and arteries. Using PI (thickness 80 μm), a thin and flexible material, as the substrate allows for designs suitable for a wide range of artery sizes and implantation locations. Characterization of the sensor's performance yielded sensitivities of $0.015 \pm 0.0035\ \mathrm{kPa}^{-1}$ at 0–3 kPa, $0.0022 \pm 0.00049\ \mathrm{kPa}^{-1}$ at 3–38 kPa, and $0.00038 \pm 0.00011\ \mathrm{kPa}^{-1}$ at 38–100 kPa. The sensors maintained stable electrical signals after tens of thousands of cycles in repeated experiments over more than 24 hours, demonstrating the repeatability and consistency of the sensor manufacturing. To verify the effect of sensor adhesion on signal enhancement, the response to pulsation in polyolefin tubes was tested, with 1 pound of artificial fat, skin, and muscle layered on the sensor surrounding the artificial artery to better simulate typical *in vivo* environments. The sensor's signal response was stronger, possibly due to tighter contact between the sensor and the polyolefin tube. This technology provides a new solution for wireless monitoring of arterial health and supports early detection and prevention of pre-symptomatic diseases. Continuous monitoring of arterial health allows doctors to identify potential issues early and take appropriate measures, effectively reducing the risk of severe diseases such as strokes and heart attacks (Fig. 10b). In addition to choosing soft materials such as PDMS and PI, hydrogels are also an excellent choice, offering effective mechanical properties for wearable devices used in healthcare. However, most hydrogel patches mixed with conductive materials exhibit uneven distribution, leading to unstable conductivity. Furthermore, most hydrogels have poor adhesion performance on wet and deformable surfaces due to the high swelling of hydrophilic polymer matrices, reducing their adhesion capability at interfaces. Therefore, hydrogels need to enhance their self-adhesiveness to ensure stable fixation on wet dynamic tissues. Recently, wet-adhesive hydrogels have advanced significantly, but these hydrogels may pose cytotoxicity risks due to *in situ* chemical crosslinking reactions and are mostly non-degradable. To

address this, Ou *et al.*[184] developed the PPG hydrogel by constructing conductive polydopamine hybrid PEDOT nanoparticles (PPEDOT NPs) and polyglutamic acid (PGA) interpenetrating gelatin methacryloyl (GelMA) networks. PEDOT NPs uniformly distributed in the polymer network form good conductive pathways. The hydrogel network structure provides hydrophilicity, enabling wet adhesion during dynamic deformations, such as heartbeats. The wet adhesion of the hydrogel is achieved through a desolvation strategy in ethanol, regulating polymer chain entanglement to form a desolvation network. When the hydrogel comes into contact with wet tissue surfaces, the desolvated network rapidly absorbs interfacial water, disrupting the hydration layer and allowing direct interactions between the adhesive groups in the hydrogel and heart tissue. Stretching tests demonstrated that the PPG hydrogel has high flexibility (fracture strain $>90\%$), softness (a Young's modulus of 138 kPa), and high fatigue resistance. In stretch-adhesion experiments, the adhesion strength of the desolvated PPG hydrogel (13 kPa) was higher than that of the PBS-swollen PPG hydrogel (5.8 kPa), confirming the importance of the desolvation process for wet adhesion performance. PPEDOT NPs establish high conductivity paths in the hydrogel network and create a dynamic redox balance system of phenol and quinone groups, where oxidation and reduction correspond to phenol to quinone transitions. The PDA and PEDOT in PPEDOT NPs form an electron donor–acceptor complex, maintaining a sufficient number of phenol groups, thus enhancing the long-term adhesion of the PPG hydrogel to wet pig heart tissue. The PPG hydrogel also exhibits adhesion to various wet substrates (*e.g.*, glass slides (7 kPa), stainless steel surfaces (10 kPa), fresh pig muscle (9 kPa), and PTFE substrates (22 kPa)). To further demonstrate the stable conductivity of the hydrogel, it was adhered to the wet and curved surface of an *ex vivo* pig heart and used as an adhesive electrode to record ECG signals by simulating heartbeats through pressing. The PPG hydrogel, placed in deionized water to construct a circuit for LED illumination, maintained a stable conductivity of >15 S m^{-1}, higher than that of biological tissues (0.3–0.7 S m^{-1}), validating its normal operation in wet environments and compensation for electrophysiological conduction in heart tissue. Measuring the resistance changes during compressive deformation with a GF of 0.69 reflected the mechanical sensitivity of the PPG hydrogel. Without using glue, the PPG hydrogel adhered directly to fresh pig hearts, demonstrating excellent wet adhesion, remaining firmly attached even under tap water rinsing. The polyphenol groups and RGD sequences in the PPG hydrogel interact covalently and non-covalently (hydrogen bonds and electrostatic interactions) with amino and thiol groups on tissue surfaces, achieving instant adhesion. These properties of the PPG hydrogel promote its application as an adhesive and conductive cardiac patch in myocardial infarction treatment (Fig. 10c). To further explore human cognitive abilities, it is essential to understand brain functions. Obtaining electrical signals from brain folds can contribute to the completion of neural mapping, which can be achieved through real-time monitoring using EEG electrodes, stereoelectroencephalography (SEEG) electrodes, and ECoG electrodes. Among these types, ECoG electrodes can obtain precise signals within cortical folds without causing severe brain damage. Numerous flexible ECoG monitoring electrodes have been widely reported, such as electrode arrays made from Au–TiO_2 nanowire conductors embedded in PDMS and Au–PI materials. These electrodes possess flexibility, stretchability, and high electrode density while maintaining compatibility with the cortical surface. However, due to the PDMS electrode array's substrate thickness of 80 μm, it cannot effectively cover the highly folded brain surface. Additionally, brain electrode arrays based on Au/PI materials are not very effective in monitoring ECoG signals. To address this challenge, the key lies in balancing the mechanical properties and conformal adhesion of materials and effectively controlling material thickness. To this end, Xiao *et al.*[185] developed a novel ultra-thin (2.2 μm) ECoG electrode that improves electrode flexibility by controlling material thickness to enhance conformal contact. A 2 μm-thick sacrificial layer of silicon dioxide was thermally grown on a silicon wafer, followed by spin coating of an ultra-thin PI substrate layer. A gold layer was then deposited and patterned using UV lithography and electron beam evaporation to form the metal layer. Successive spin coatings of the PI encapsulation layer and aluminum hard mask were applied. The mesh structure was etched using UV lithography, aluminum etching, and oxygen plasma dry etching methods, and the recording sites were exposed in the same manner. Finally, the electrode device was released in hydrofluoric acid and transferred onto a silk membrane. Additionally, a water-soluble silk membrane was used as the support layer, making the ultra-thin device easier to handle and ensuring that it could wrap around and adhere firmly to the brain's folds once the membrane dissolved, achieving comprehensive neural mapping. After completing the fabrication and assembly of the ultra-thin brain electrode device, it was applied to different animal brain models (from cats to sheep, with increasing complexity and number of sulci). By comparing the conformal attachment of the brain surface with sulci to the normal attachment area, the effectiveness of the conformal attachment achieved through specific treatments of the electrode materials was demonstrated, offering new opportunities for diagnosing and treating various neurological diseases (Fig. 10d). To adapt to the wet environment of the human body, the wet adhesion of wearable devices can be improved by selecting moisture-compatible materials, constructing micro/nano-structures and building network crosslinking structures. These strategies offer new avenues for the application of wearable devices in the human body. In addition to better fitting and adhering to internal organs or tissues, the wettability design of materials can significantly enhance the ability of wearable devices to adapt to fluid environments. For example, depositing a thick and dense hydrophobic layer on hydrophilic fabrics, nanofibers, and hydrogels can make it a waterproof outer layer for devices. In daily life, it is inevitable to sustain skin wounds caused by sharp objects. To better treat wounds, controlling bleeding and removing excess biological fluids (such as wound exudate,

sweat, and urine) is usually necessary. Accumulation of biological fluids around wounds often causes infection, hindering healing. However, traditional hydrophilic dressings have unique hydrophilicity that can absorb some biological fluids, but they inevitably leave biological fluids at the wound–skin interface. This indicates that the surface wettability of wound dressings usually affects the wettability behavior of biological fluids around the wound. Most traditional dressings are made of hydrophilic materials that are easily wetted by biological fluids, resulting in overhydration of the wound. In contrast, a hydrophobic material coated on the outer layer of the dressing acts as a waterproof layer, preventing accidental contact of external fluids with the wound but not promoting the removal of biological fluids. Recently, several materials with asymmetric wettability have demonstrated unique water droplet transfer capabilities, such as polyester fabrics with wettability gradients, PU/polyvinyl chloride composite fiber membranes, and single-sided fluorinated cotton fabric membranes. Due to the low cost and flexible, durable network structure of medical gauze, it is traditionally used as a wound dressing. Its cotton microfibers interpenetrate, forming a super-hydrophilic network. PU, a hydrophobic, biocompatible medical material, also has easy processing characteristics. Therefore, Wang *et al.*[186] constructed a self-pumping dressing by electrospinning hydrophobic PU nanofiber arrays onto the cotton microfibers of a hydrophilic medical gauze. To demonstrate the one-way drainage capability of the self-pumping dressing, green fetal bovine serum (FBS) droplets were added. When the droplets came into contact with the hydrophobic layer, they were pumped through to wet the hydrophilic layer. When the droplets came into contact with the hydrophilic layer, they quickly wetted it but were blocked by the hydrophobic layer. As FBS continued to drip in, the self-pumping process proceeded one-way from the hydrophobic side to the hydrophilic side. This process occurs because when liquid droplets land on the self-pumping dressing's hydrophobic nanofibers, the liquid comes into contact with multiple contact points of the hydrophilic microfibers and the wetting force drives the fluid to wet the hydrophilic microfiber network. This self-pumping dressing can one-way absorb excess biological fluids from the hydrophobic side to the hydrophilic side, preventing biological fluids from wetting the wound. To explore the wetting behavior of water droplets on hydrophobic PU nanofiber arrays, 2 μL of water droplets were dropped onto low-density ($6.7 \pm 1.5\%$) hydrophobic nanofiber arrays. The droplets seemed to partially penetrate the hydrophobic nanofiber arrays and maintained a perfect spherical shape (CA $\approx 146^{\circ}$), indicating that higher hydrophobic nanofiber density makes water droplets harder to penetrate. Therefore, controlling the density of the hydrophobic nanofiber arrays can regulate water droplet penetration. In practical applications, the hydrophobic layer should serve as the wound contact layer to effectively drain excess biological fluids (Fig. 10e). Under normal circumstances, implantable wearable electronic devices face the wet environment inside the human body, so it is necessary to carry out wettability design on the material surface. For example, by mimicking the Janus structure to prevent potential bacterial infections, one side can be designed as a low adhesion or super hydrophobic surface, using droplet rolling to clean surface particles, providing excellent water resistance and preventing device damage. The other side can be treated with a strong adhesive according to the texture of the organ or tissue to ensure the biocompatibility of the flexible electronic products in the body and extend the service life of the equipment. The construction of an equal gradient wetting interface can also play a role in adapting to the body's wettability environment.

6 Conclusion and outlook

In this review, we innovatively approach the field of conformal and human-adaptive electronic devices from the perspective of surface engineering, delving into the latest breakthroughs, particularly focusing on the fine-tuning strategies of surface adhesion and wettability in wearable devices. The core of this strategy lies in the meticulous design of material wettability. This includes adjusting surface wettability properties by applying hydrophobic or hydrophilic coatings or constructing micro/nano-scale structures to alter surface roughness, thereby regulating wettability. Moreover, plasma treatment technology can significantly modify the chemical properties of the material surface, achieving precise wettability control. These measures aim to optimize the wettability behavior of wearable device substrates and encapsulation materials, ensuring stable and close wetting connections with the skin or other contact interfaces in humid or underwater environments (such as rain or sweat-soaked scenarios). This greatly reduces signal noise and interference, significantly enhancing the quality and reliability of signal acquisition, which is invaluable for accurately capturing physiological indicators such as heart rate and electromyographic signals. Given the inherent complexity and variability of the human skin surface, including natural features like wrinkles and hair, ensuring that the devices adapt flexibly and conform closely to these irregular surfaces presents a significant challenge. To address this, we explore a variety of innovative strategies such as precisely controlling device thickness, ingeniously constructing bio-inspired micro/nano-structures (drawing inspiration from the strong adhesion mechanisms of gecko feet and octopus suckers), designing nano-network structures, and skillfully integrating functional fillers into polymer matrices. These approaches aim to multi-dimensionally regulate the surface adhesion of materials to achieve conformal contact, ensuring that the devices seamlessly integrate and conform to these complex and variable surfaces while maintaining comfort and stability during prolonged wear. Our research centers on the synergistic optimization of wettability and adhesion, aiming to enhance the adaptive adhesion and wettability regulation capabilities of wearable devices across diverse human organs/tissues (such as the face, hands, eyes, joints, as well as blood vessels, heart, muscles, and brain), thereby providing a solid foundation for precise monitoring of physiological and biochemical signals.

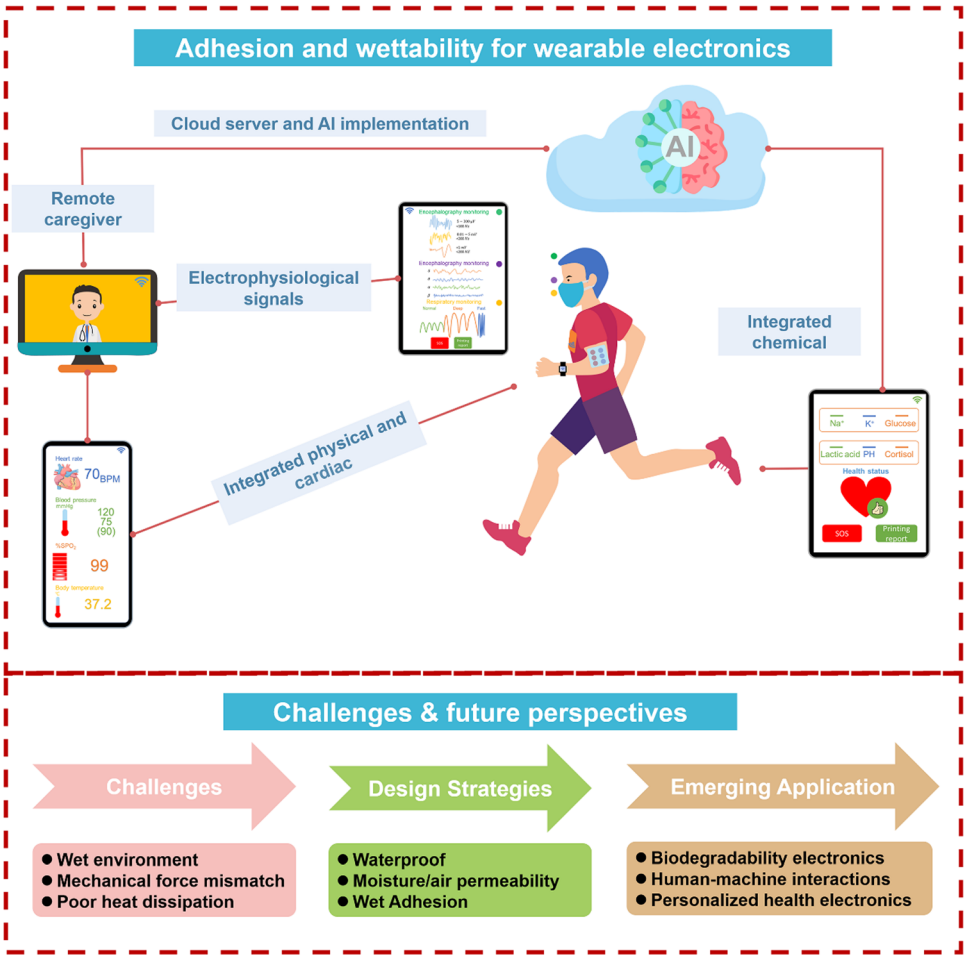

Fig. 11 Monitoring signals generated from various parts of the human body using wearable electronics and their corresponding challenges and future perspectives.

To this end, we visually present the signal monitoring capabilities of wearable devices on different interfaces inside and outside the human body through Fig. 11, profoundly revealing the current challenges, coping strategies, and future directions.

However, we must soberly recognize that research on conformal and human-adaptive electronic devices is still in its infancy. Despite numerous pioneering studies and proof-of-concept demonstrations, promoting their commercialization still requires overcoming numerous hurdles, especially the deep-level challenges in the regulation and design of surface adhesion and wettability. Next, we will delve into these specific issues, aiming to identify the bottlenecks in current research and inspire more innovative ideas and solutions from researchers to collectively drive the flourishing development of the flexible electronics field.

(I) Water-soluble polymers, owing to the abundance of hydrophilic groups (including cationic, anionic, and polar nonionic groups) in their molecular structure, can easily dissolve or swell in water, forming stable aqueous solutions or dispersion systems. This characteristic endows them with unique advantages in the field of wearable devices: good hydrophilicity and biocompatibility make these polymers ideal for long-term contact with human skin, effectively reducing the risk of irritation and allergic reactions. However, when used as substrates or encapsulation materials for wearable devices, the sweat generated during the wearer's physical activities poses a challenge. The infiltration of sweat may lead to the degradation of the water-soluble polymer substrate, thereby affecting the accuracy and reliability of the monitoring signals and even causing device failure or damage. To address this issue, material selection becomes crucial. Considering the introduction of hydrophobic and flexible materials (such as PDMS, Ecoflex, *etc.*) as substrates for wearable devices, these materials not only maintain excellent performance under substantial external force or frequent friction but also confer waterproof characteristics to the device, thereby effectively extending its service life. This strategy not only solves the stability problem of water-soluble polymers in humid environments but also enhances the overall durability and practicality of wearable devices.

(II) Commonly used substrate materials for wearable devices, such as PDMS, PU, and PI, generally face the issue of poor breathability. When these materials are used as substrates for wearable devices and tightly fit the human skin, their low breathability hinders the smooth discharge of sweat, leading to

sweat accumulation at the contact interface, which may infiltrate the device, causing corrosion and damage. Additionally, the heat generated during the long-term operation of wearable devices, due to poor breathability, cannot be effectively dissipated to the outside, increasing the risk of skin burns for the wearer. To solve this problem, there is an urgent need to explore substrate materials with better breathability. Textiles, with their unique porous structure, become a promising choice. Using textiles as substrate materials for wearable devices can significantly enhance the breathability of the devices, effectively preventing sweat accumulation and infiltration. Furthermore, carefully designing the material surface wettability, by constructing gradient wettability interfaces or asymmetric Janus structures, can further optimize the process of rapid sweat transport and evaporation. This design can accelerate the flow of sweat on the material surface, promoting rapid evaporation of sweat, thereby reducing heat accumulation at the contact interface and maintaining dryness and comfort of the interface. Such innovations not only solve the problem of poor breathability of wearable devices but also improve the comfort of the wearer and the overall performance of the devices.

(III) Ensuring an appropriate balance of adhesion between wearable devices and the contact interfaces inside and outside the human body is a major challenge in device design. Excessive adhesion can cause significant mechanical stress and pulling force on the skin when removing or moving the device, leading to epidermal tearing, abrasion, or peeling, which is particularly detrimental to sensitive or fragile skin. Moreover, strong adhesion can compress the skin, affecting breathability and blood circulation, causing the skin to become moist, red, and swollen and even inducing skin lesions. Conversely, if the adhesion is too weak, wearable devices may not securely fit the skin, leading to unstable and inaccurate monitoring signals. This is especially critical in healthcare and health monitoring fields, where the accuracy and stability of signals are directly related to disease diagnosis and prevention. Therefore, researchers must pay close attention to the adhesion properties of materials when designing wearable devices to ensure user comfort while guaranteeing accurate monitoring signals. To this end, surface treatment strategies such as constructing micro/nano-structures, designing nano-network structures, or optimizing device thickness can effectively regulate the adhesion between the material and the skin interface, achieving an ideal adhesion balance.

(IV) During physical activities, the secretion of sweat on the skin surface significantly reduces the shear viscosity in the region, which may weaken the adhesion of wearable devices, even leading to device detachment from the skin interface, thus weakening signal strength and reducing data reliability. Moreover, the accumulation of sweat at the interface between the wearable device electrodes and the skin provides an ideal environment for bacterial growth (such as proteins, amino acids, *etc.*), which over time, softens the stratum corneum of the skin, weakening its natural barrier function, making the skin more susceptible to microbial invasion and infection, thereby increasing the risk of skin infections. Therefore, researchers must pay special attention to the biocompatibility and antibacterial ability of materials when designing wearable devices. To effectively address the problems caused by sweat accumulation, an innovative design approach is to adopt an asymmetric Janus structure. Specifically, this involves designing the hydrophobic side of the material to be in direct contact with the skin to repel sweat, while the other side adopts a hydrophilic material, placed externally to better handle or direct sweat. This carefully designed structure not only reduces sweat accumulation but also effectively exerts antibacterial effects, providing safety guarantee for the long-term use of wearable devices.

(V) Wearable devices play a key role in health monitoring and therapeutic diagnostics, so ensuring the accuracy and stability of monitoring signals is crucial. However, during long-term health monitoring, inevitable body movements and physiological activities (such as walking, running, breathing, heartbeat, *etc.*) can interfere with signal measurement. Even external environmental factors (such as device movement or vibration) can introduce motion artifacts, severely affecting the quality of bioelectrical signals, leading to distorted monitoring data, which threatens the accuracy of health assessments and diagnostics. To address this problem, multiple aspects need to be considered. First, material selection is key, with priority given to materials that match the mechanical properties of tissues (such as softness and stretchability) to reduce interface instability caused by mechanical mismatches between the device and biological tissues. Secondly, optimizing material structure design, such as adopting ultra-thin, strain-adjustable, and stretchable designs, can significantly enhance the device's adaptability to dynamic tissue changes, effectively reducing interface impedance fluctuations. Finally, from the perspective of surface engineering, strategies such as introducing microstructured surfaces or using physical/chemical adhesives can enhance the adhesion between wearable devices and biological tissues, ensuring long-term stability at the contact interface, thereby further improving the accuracy and reliability of monitoring signals.

Addressing the shortcomings and challenges faced by wearable devices from the perspective of surface engineering, wettability design and interface adhesion optimization are key breakthroughs to enhance their performance. Wettability design, through the fine-tuning of surface hydrophilicity and hydrophobicity, effectively enhances the stability and reliability of devices in complex physiological environments, significantly reducing the risk of performance degradation due to liquid residue formation or infiltration. Simultaneously, interface adhesion optimization, through innovations in micro/nano-structures, the application of high-performance adhesives, and the development of smart adhesive materials ensure the firm adherence of devices in dynamic human environments, significantly reducing signal interference and data distortion caused by detachment or displacement. These strategies pave new ways for researchers, aiding in the development of multifunctional wearable devices that integrate precise and stable

signal monitoring and waterproof and self-cleaning properties, further promoting their extensive applications and rapid development in advanced fields such as healthcare, personalized health monitoring, instant diagnostics, and human–machine interaction. Although wearable devices have made significant progress in the medical field, their potential remains vast and yet to be fully explored. To achieve a high degree of conformity and perfect adaptation between wearable devices and the human body, characteristics such as lightweight design, excellent durability, wireless connectivity, waterproof stability, and reversible adhesion ability are considered indispensable. Looking forward, research will focus on developing more sensitive sensor technologies, promoting the deep integration of data transmission and machine learning technologies, and constructing real-time monitoring systems for personal health status, thereby empowering a new era of proactive health management. This in-depth discussion not only reviews and broadens the research horizons of wearable devices but also lays a solid theoretical and practical foundation for achieving the grand blueprint of personalized and proactive health management.

Author contributions

Wenfu Chen: investigation, writing – original draft; Junzhu Lin: investigation, writing – reviewing and editing; Zhicheng Ye: investigation, writing – reviewing and editing; Xiangyu Wang: writing – reviewing and editing; Jie Shen: writing – reviewing and editing; and Ben Wang: Project administration, conceptualization, funding acquisition, writing – reviewing and editing.

Data availability

The data that support the findings of this review are available upon request from the corresponding author.

Conflicts of interest

The authors declare no competing interests.

Acknowledgements

This work was supported by the National Natural Science Foundation of China (22102104), Natural Science Foundation of Shenzhen Science and Technology Commission with grant no. RCBS20200714114920190 and JCYJ20220531103409021, and Guangdong Basic and Applied Basic Research Foundation (2021A1515010672).

References

1 M. Amjadi, K.-U. Kyung, I. Park and M. Sitti, *Adv. Funct. Mater.*, 2016, **26**, 1678–1698.
2 H. Chen, Y. Song, X. Cheng and H. Zhang, *Nano Energy*, 2019, **56**, 252–268.
3 P. Chen, X. Sun and H. Peng, *Adv. Funct. Mater.*, 2020, **30**, 2001827.
4 H. Chu, H. Jang, Y. Lee, Y. Chae and J.-H. Ahn, *Nano Energy*, 2016, **27**, 298–305.
5 N. Gogurla, B. Roy, J.-Y. Park and S. Kim, *Nano Energy*, 2019, **62**, 674–681.
6 F. He, X. You, H. Gong, Y. Yang, T. Bai, W. Wang, W. Guo, X. Liu and M. Ye, *ACS Appl. Mater. Interfaces*, 2020, **12**, 6442–6450.
7 Y. Khan, A. E. Ostfeld, C. M. Lochner, A. Pierre and A. C. Arias, *Adv. Mater.*, 2016, **28**, 4373–4395.
8 J. Kim, Y. Lee, M. Kang, L. Hu, S. Zhao and J. H. Ahn, *Adv. Mater.*, 2021, **33**, 2005858.
9 G. H. Lee, H. Kang, J. W. Chung, Y. Lee, H. Yoo, S. Jeong, H. Cho, J.-Y. Kim, S.-G. Kang, J. Y. Jung, S. G. Hahm, J. Lee, I.-J. Jeong, M. Park, G. Park, I. H. Yun, J. Y. Kim, Y. Hong, Y. Yun, S.-H. Kim and B. K. Choi, *Sci. Adv.*, 2022, **8**, eabm3622.
10 J. Li, P. Yang, X. Li, C. Jiang, J. Yun, W. Yan, K. Liu, H. J. Fan and S. W. Lee, *ACS Energy Lett.*, 2023, **8**, 1–8.
11 S. Wang, J. Xu, W. Wang, G.-J. N. Wang, R. Rastak, F. Molina-Lopez, J. W. Chung, S. Niu, V. R. Feig, J. Lopez, T. Lei, S.-K. Kwon, Y. Kim, A. M. Foudeh, A. Ehrlich, A. Gasperini, Y. Yun, B. Murmann, J. B. H. Tok and Z. Bao, *Nature*, 2018, **555**, 83–88.
12 X. Wu, W. Ren, Y. Wen, S. Ono, J. Zhu, J. W. Evans and A. C. Arias, *ACS Sens.*, 2023, **8**, 2740–2749.
13 C. Xu, Y. Yang and W. Gao, *Matter*, 2020, **2**, 1414–1445.
14 Y. Yin, Y. Cui, Y. Li, Y. Xing and M. Li, *Appl. Therm. Eng.*, 2018, **144**, 504–511.
15 D. B. Ahn, S.-S. Lee, K.-H. Lee, J.-H. Kim, J.-W. Lee and S.-Y. Lee, *Energy Storage Mater.*, 2020, **29**, 92–112.
16 A. E. Ali, V. Jeoti and G. M. Stojanovic, *Sci. Technol. Adv. Mater.*, 2021, **22**, 772–793.
17 B. Bozali, S. Ghodrat and K. M. B. Jansen, *Micromachines*, 2023, **14**, 710.
18 S. Cho, T. Chang, T. Yu and C. H. Lee, *Biosens.*, 2022, **12**, 222.
19 R. Das, W. Zeng, C. Asci, R. Del-Rio-Ruiz and S. Sonkusale, *APL Bioeng.*, 2022, **6**, 021505.
20 W. Gao, H. Ota, D. Kiriya, K. Takei and A. Javey, *Acc. Chem. Res.*, 2019, **52**, 523–533.
21 J. Kim, J. Lee, D. Son, M. K. Choi and D. H. Kim, *Nano Converge.*, 2016, **3**, 4.
22 L. W. Lo, J. Zhao, K. Aono, W. Li, Z. Wen, S. Pizzella, Y. Wang, S. Chakrabartty and C. Wang, *ACS Nano*, 2022, **16**, 11792–11801.
23 A. Mahmoudi Khomami and F. Najafi, *Rob. Autom. Syst.*, 2021, **144**, 103846.
24 C. Park, M. S. Kim, H. H. Kim, S.-H. Sunwoo, D. J. Jung, M. K. Choi and D.-H. Kim, *Appl. Phys. Rev.*, 2022, **9**, 021312.
25 X. Sun, C. Zhao, H. Li, H. Yu, J. Zhang, H. Qiu, J. Liang, J. Wu, M. Su, Y. Shi and L. Pan, *Micromachines*, 2022, **13**, 784.
26 S. Wang, Q. Xu and H. Sun, *Adv. Fiber Mater.*, 2022, **4**, 324–341.

27 Y. Wang, S. Gong, S. J. Wang, G. P. Simon and W. Cheng, *Mater. Horiz.*, 2016, **3**, 208–213.
28 Q. Qiu, M. Zhu, Z. Li, K. Qiu, X. Liu, J. Yu and B. Ding, *Nano Energy*, 2019, **58**, 750–758.
29 Q. Shen, X. Yang, L. Zou, K. Wei, C. Wang and G. Liu, *IEEE Internet Things J.*, 2022, **9**, 25207–25222.
30 G. Wang, T. Liu, X.-C. Sun, P. Li, Y.-S. Xu, J.-G. Hua, Y.-H. Yu, S.-X. Li, Y.-Z. Dai, X.-Y. Song, C. Lv and H. Xia, *Sens. Actuators, A*, 2018, **280**, 319–325.
31 K. Chen, Y. Hu, M. Liu, F. Wang, P. Liu, Y. Yu, Q. Feng and X. Xiao, *Macromol. Mater. Eng.*, 2021, **306**, 2100341.
32 H. Huang, Y. Feng, X. Yang and Y. Shen, *Biosens. Bioelectron.*, 2022, **214**, 114547.
33 N. Li, S. Gao, Y. Li, J. Liu, W. Song and G. Shen, *Nano Res.*, 2023, **16**, 7583–7592.
34 Y. Q. Liu, J. R. Zhang, D. D. Han, Y. L. Zhang and H. B. Sun, *ACS Appl. Mater. Interfaces*, 2019, **11**, 38084–38091.
35 L. Wang, K. Jiang and G. Shen, *Appl. Phys. Lett.*, 2021, **119**, 150501.
36 S. Xia, W. Fu, J. Liu and G. Gao, *Sci. China: Mater.*, 2023, **66**, 2843–2851.
37 L. Xie, Z. Zhang, Q. Wu, Z. Gao, G. Mi, R. Wang, H. B. Sun, Y. Zhao and Y. Du, *Nanoscale*, 2023, **15**, 405–433.
38 T. An, D. V. Anaya, S. Gong, L. W. Yap, F. Lin, R. Wang, M. R. Yuce and W. Cheng, *Nano Energy*, 2020, **77**, 105295.
39 S. Chen, N. Wu, S. Lin, J. Duan, Z. Xu, Y. Pan, H. Zhang, Z. Xu, L. Huang, B. Hu and J. Zhou, *Nano Energy*, 2020, **70**, 104460.
40 J. Gao, Y. Fan, Q. Zhang, L. Luo, X. Hu, Y. Li, J. Song, H. Jiang, X. Gao, L. Zheng, W. Zhao, Z. Wang, W. Ai, Y. Wei, Q. Lu, M. Xu, Y. Wang, W. Song, X. Wang and W. Huang, *Adv. Mater.*, 2022, **34**, 2107511.
41 Y. Gao, L. Yu, J. C. Yeo and C. T. Lim, *Adv. Mater.*, 2020, **32**, 1902133.
42 Y. J. Hong, H. Jeong, K. W. Cho, N. Lu and D. H. Kim, *Adv. Funct. Mater.*, 2019, **29**, 1808247.
43 S. H. Lee, Y. S. Kim and W. H. Yeo, *Adv. Healthcare Mater.*, 2021, **10**, 2101400.
44 M. Liao, H. Liao, J. Ye, P. Wan and L. Zhang, *ACS Appl. Mater. Interfaces*, 2019, **11**, 47358–47364.
45 R. Yin, D. Wang, S. Zhao, Z. Lou and G. Shen, *Adv. Funct. Mater.*, 2021, **31**, 2008936.
46 N. Zhang, Y. Li, S. Xiang, W. Guo, H. Zhang, C. Tao, S. Yang and X. Fan, *Nano Energy*, 2020, **72**, 104664.
47 A. Miyamoto, S. Lee, N. F. Cooray, S. Lee, M. Mori, N. Matsuhisa, H. Jin, L. Yoda, T. Yokota, A. Itoh, M. Sekino, H. Kawasaki, T. Ebihara, M. Amagai and T. Someya, *Nat. Nanotechnol.*, 2017, **12**, 907–913.
48 K. He, Z. Liu, C. Wan, Y. Jiang, T. Wang, M. Wang, F. Zhang, Y. Liu, L. Pan, M. Xiao, H. Yang and X. Chen, *Adv. Mater.*, 2020, **32**, 2001130.
49 W. Jeong, J. Song, J. Bae, K. R. Nandanapalli and S. Lee, *ACS Appl. Mater. Interfaces*, 2019, **11**, 44758–44763.
50 Y. R. Jeong, G. Lee, H. Park and J. S. Ha, *Acc. Chem. Res.*, 2019, **52**, 91–99.
51 Z. Lou, L. Wang, K. Jiang, Z. Wei and G. Shen, *Mater. Sci. Eng., R*, 2020, **140**, 100523.
52 H. Luo and B. Gao, *Eng. Regen.*, 2021, **2**, 163–170.
53 S. Chen, Z. Qiao, Y. Niu, J. C. Yeo, Y. Liu, J. Qi, S. Fan, X. Liu, J. Y. Lee and C. T. Lim, *Nat. Rev. Bioeng.*, 2023, **1**, 950–971.
54 B. Lemaire, Y. Yu, N. Molinari, H. Wu, Z. A. H. Goodwin, F. Stricker, B. Kozinsky and J. Aizenberg, *Proc. Natl. Acad. Sci. U. S. A.*, 2023, **120**, e2308804120.
55 M. Li, C. Li, B. R. K. Blackman and S. Eduardo, *Int. Mater. Rev.*, 2022, **67**, 658–681.
56 F. Gao, C. Liu, L. Zhang, T. Liu, Z. Wang, Z. Song, H. Cai, Z. Fang, J. Chen, J. Wang, M. Han, J. Wang, K. Lin, R. Wang, M. Li, Q. Mei, X. Ma, S. Liang, G. Gou and N. Xue, *Microsyst. Nanoeng.*, 2023, **9**, 1.
57 J. T. Reeder, J. Choi, Y. Xue, P. Gutruf, J. Hanson, M. Liu, T. Ray, A. J. Bandodkar, R. Avila, W. Xia, S. Krishnan, S. Xu, K. Barnes, M. Pahnke, R. Ghaffari, Y. Huang and J. A. Rogers, *Sci. Adv.*, 2019, **5**, eaau6356.
58 Y. Mao, Y. Zhu, T. Zhao, C. Jia, M. Bian, X. Li, Y. Liu and B. Liu, *Biosens.*, 2021, **11**, 147.
59 H. Zhu, H. Yang, L. Zhan, Y. Chen, J. Wang and F. Xu, *ACS Sens.*, 2022, **7**, 3014–3022.
60 S. R. A. Ruth, M. G. Kim, H. Oda, Z. Wang, Y. Khan, J. Chang, P. M. Fox and Z. Bao, *iScience*, 2021, **24**, 103079.
61 V. Kalidasan, X. Yang, Z. Xiong, R. R. Li, H. Yao, H. Godaba, S. Obuobi, P. Singh, X. Guan, X. Tian, S. A. Kurt, Z. Li, D. Mukherjee, R. Rajarethinam, C. S. Chong, J. W. Wang, P. L. R. Ee, W. Loke, B. C. K. Tee, J. Ouyang, C. J. Charles and J. S. Ho, *Nat. Biomed. Eng.*, 2021, **5**, 1217–1227.
62 J. Zhong, Z. Li, M. Takakuwa, D. Inoue, D. Hashizume, Z. Jiang, Y. Shi, L. Ou, M. O. G. Nayeem, S. Umezu, K. Fukuda and T. Someya, *Adv. Mater.*, 2022, **34**, 2107758.
63 P. Escobedo, M. D. Fernandez-Ramos, N. Lopez-Ruiz, O. Moyano-Rodriguez, A. Martinez-Olmos, I. M. Perez de Vargas-Sansalvador, M. A. Carvajal, L. F. Capitan-Vallvey and A. J. Palma, *Nat. Commun.*, 2022, **13**, 72.
64 B. Mirani, Z. Hadisi, E. Pagan, S. M. H. Dabiri, A. van Rijt, L. Almutairi, I. Noshadi, D. G. Armstrong and M. Akbari, *Adv. Healthcare Mater.*, 2023, **12**, 2203233.
65 B. Xu, A. Akhtar, Y. Liu, H. Chen, W. H. Yeo, S. I. Park, B. Boyce, H. Kim, J. Yu, H. Y. Lai, S. Jung, Y. Zhou, J. Kim, S. Cho, Y. Huang, T. Bretl and J. A. Rogers, *Adv. Mater.*, 2016, **28**, 4462–4471.
66 S. Zheng, W. Li, Y. Ren, Z. Liu, X. Zou, Y. Hu, J. Guo, Z. Sun and F. Yan, *Adv. Mater.*, 2022, **34**, 2106570.
67 Q. Han, C. Zhang, T. Guo, Y. Tian, W. Song, J. Lei, Q. Li, A. Wang, M. Zhang, S. Bai and X. Yan, *Adv. Mater.*, 2023, **35**, 2209606.
68 J. Alberto, C. Leal, C. Fernandes, P. A. Lopes, H. Paisana, A. T. de Almeida and M. Tavakoli, *Sci. Rep.*, 2020, **10**, 5539.
69 J.-H. Kim, C. Marcus, R. Ono, D. Sadat, A. Mirzazadeh, M. Jens, S. Fernandez, S. Zheng, T. Durak and C. Dagdeviren, *Nat. Electron.*, 2022, **5**, 794–807.

70 Y. Jiang, A. A. Trotsyuk, S. Niu, D. Henn, K. Chen, C. C. Shih, M. R. Larson, A. M. Mermin-Bunnell, S. Mittal, J. C. Lai, A. Saberi, E. Beard, S. Jing, D. Zhong, S. R. Steele, K. Sun, T. Jain, E. Zhao, C. R. Neimeth, W. G. Viana, J. Tang, D. Sivaraj, J. Padmanabhan, M. Rodrigues, D. P. Perrault, A. Chattopadhyay, Z. N. Maan, M. C. Leeolou, C. A. Bonham, S. H. Kwon, H. C. Kussie, K. S. Fischer, G. Gurusankar, K. Liang, K. Zhang, R. Nag, M. P. Snyder, M. Januszyk, G. C. Gurtner and Z. Bao, *Nat. Biotechnol.*, 2023, **41**, 652–662.
71 L. Tang, J. Shang and X. Jiang, *Sci. Adv.*, 2021, **7**, eabe3778.
72 J. Wang, L. Wang, G. Li, D. Yan, C. Liu, T. Xu and X. Zhang, *ACS Sens.*, 2022, **7**, 3102–3107.
73 K. Kim, H. J. Kim, H. Zhang, W. Park, D. Meyer, M. K. Kim, B. Kim, H. Park, B. Xu, P. Kollbaum, B. W. Boudouris and C. H. Lee, *Nat. Commun.*, 2021, **12**, 1544.
74 S. Duan, Y. Lin, C. Zhang, Y. Li, D. Zhu, J. Wu and W. Lei, *Nano Energy*, 2022, **91**, 106650.
75 J. Yang, Z. Zhang, P. Zhou, Y. Zhang, Y. Liu, Y. Xu, Y. Gu, S. Qin, H. Haick and Y. Wang, *Nanoscale*, 2023, **15**, 3051–3078.
76 X. Wang, Y. Liu, H. Cheng and X. Ouyang, *Adv. Funct. Mater.*, 2022, **32**, 2200260.
77 S. Gong, Y. Lu, J. Yin, A. Levin and W. Cheng, *Chem. Rev.*, 2024, **124**, 455–553.
78 Y. Niu, H. Liu, R. He, Z. Li, H. Ren, B. Gao, H. Guo, G. M. Genin and F. Xu, *Mater. Today*, 2020, **41**, 219–242.
79 S. M. A. Iqbal, I. Mahgoub, E. Du, M. A. Leavitt and W. Asghar, *npj Flexible Electron.*, 2021, **5**, 9.
80 D. R. Seshadri, R. T. Li, J. E. Voos, J. R. Rowbottom, C. M. Alfes, C. A. Zorman and C. K. Drummond, *npj Digit. Med.*, 2019, **2**, 72.
81 P. Zhu, H. Peng and A. Y. Rwei, *Med. Novel Technol. Dev.*, 2022, **14**, 100118.
82 S. Huang, Y. Liu, Y. Zhao, Z. Ren and C. F. Guo, *Adv. Funct. Mater.*, 2019, **29**, 1805924.
83 C. Cui and W. Liu, *Prog. Polym. Sci.*, 2021, **116**, 101388.
84 C. Zhang, G. R. Merana, T. Harris-Tryon and T. C. Scharschmidt, *Mucosal Immunol.*, 2022, **15**, 551–561.
85 D. Mijaljica, J. P. Townley, F. Spada and I. P. Harrison, *Prog. Lipid Res.*, 2024, **93**, 101264.
86 J. C. Yang, S. Lee, B. S. Ma, J. Kim, M. Song, S. Y. Kim, D. W. Kim, T.-S. Kim and S. Park, *Sci. Adv.*, 2022, **8**, eabn3863.
87 X. Pan, Z. Xu, R. Bao and C. Pan, *Adv. Sensor Res.*, 2023, **2**, 2300065.
88 S. Chun, D. W. Kim, S. Baik, H. J. Lee, J. H. Lee, S. H. Bhang and C. Pang, *Adv. Funct. Mater.*, 2018, **28**, 1805224.
89 S. Gupta, W. T. Navaraj, L. Lorenzelli and R. Dahiya, *npj Flexible Electron.*, 2018, **2**, 8.
90 Z. Zhang, J. Yang, H. Wang, C. Wang, Y. Gu, Y. Xu, S. Lee, T. Yokota, H. Haick, T. Someya and Y. Wang, *Sci. Adv.*, 2024, **10**, eadj5389.
91 X. Su, W. Xie, P. Wang, Z. Tian, H. Wang, Z. Yuan, X. Liu and J. Huang, *Mater. Horiz.*, 2021, **8**, 2199–2207.
92 Y. Wang, H. Hu, J. Shao and Y. Ding, *ACS Appl. Mater. Interfaces*, 2014, **6**, 2213–2218.
93 L. Hu, P. L. Chee, S. Sugiarto, Y. Yu, C. Shi, R. Yan, Z. Yao, X. Shi, J. Zhi, D. Kai, H. D. Yu and W. Huang, *Adv. Mater.*, 2023, **35**, 2205326.
94 Z. Wang, X. Wan and S. Wang, *Chem*, 2023, **9**, 771–783.
95 Y. Guo, L. Zhang, Y. Wang, J. Liang, X. Liu, Y. Jiang, L. Jiang and H. Chen, *Sci. Adv.*, 2023, **9**, eadi4843.
96 Y. Huang, T. Araki, N. Kurihira, T. Kasuga, T. Sekitani, M. Nogi and H. Koga, *Adv. Mater. Interfaces*, 2023, **10**, 2202263.
97 J. C. Yang, J. Mun, S. Y. Kwon, S. Park, Z. Bao and S. Park, *Adv. Mater.*, 2019, **31**, 1904765.
98 K. Yamagishi, S. Takeoka and T. Fujie, *Biomater. Sci.*, 2019, **7**, 520–531.
99 S. Kabiri Ameri, R. Ho, H. Jang, L. Tao, Y. Wang, L. Wang, D. M. Schnyer, D. Akinwande and N. Lu, *ACS Nano*, 2017, **11**, 7634–7641.
100 B. Ying, R. Z. Chen, R. Zuo, J. Li and X. Liu, *Adv. Funct. Mater.*, 2021, **31**, 2104665.
101 C. Pang, J. H. Koo, A. Nguyen, J. M. Caves, M. G. Kim, A. Chortos, K. Kim, P. J. Wang, J. B. H. Tok and Z. Bao, *Adv. Mater.*, 2015, **27**, 634–640.
102 F. Chen, Q. Zhuang, Y. Ding, C. Zhang, X. Song, Z. Chen, Y. Zhang, Q. Mei, X. Zhao, Q. Huang and Z. Zheng, *Adv. Mater.*, 2023, **35**, 2305630.
103 D. W. Kim, H. Kim, G.-T. Hwang, S. B. Cho, S. H. Jeon, H. W. Kim, C. K. Jeong, S. Chun and C. Pang, *ACS Energy Lett.*, 2022, **7**, 1820–1827.
104 Z. Yang, Z. Zhai, Z. Song, Y. Wu, J. Liang, Y. Shan, J. Zheng, H. Liang and H. Jiang, *Adv. Mater.*, 2020, **32**, 1907495.
105 K. Zhang, X. Shi, H. Jiang, K. Zeng, Z. Zhou, P. Zhai, L. Zhang and H. Peng, *Nat. Protoc.*, 2024, **19**, 1557–1589.
106 T. Jia, Y. Wang, Y. Dou, Y. Li, M. Jung de Andrade, R. Wang, S. Fang, J. Li, Z. Yu, R. Qiao, Z. Liu, Y. Cheng, Y. Su, M. Minary-Jolandan, R. H. Baughman, D. Qian and Z. Liu, *Adv. Funct. Mater.*, 2019, **29**, 1808241.
107 Y. K. Lee, K. I. P. Jang, Y. Ma, A. P. Koh, H. Chen, H. N. Jung, Y. Kim, J. W. Kwak, L. D. Wang, Y. Xue, Y. Yang, W. Tian, Y. Jiang, Y. P. Zhang, X. P. Feng, Y. P. Huang and J. A. P. Rogers, *Adv. Funct. Mater.*, 2017, **27**, 1605476.
108 J. A. Fan, W. H. Yeo, Y. Su, Y. Hattori, W. Lee, S. Y. Jung, Y. Zhang, Z. Liu, H. Cheng, L. Falgout, M. Bajema, T. Coleman, D. Gregoire, R. J. Larsen, Y. Huang and J. A. Rogers, *Nat. Commun.*, 2014, **5**, 3266.
109 H. Min, S. Jang, D. W. Kim, J. Kim, S. Baik, S. Chun and C. Pang, *ACS Appl. Mater. Interfaces*, 2020, **12**, 14425–14432.
110 K. I. Jang, H. U. Chung, S. Xu, C. H. Lee, H. Luan, J. Jeong, H. Cheng, G. T. Kim, S. Y. Han, J. W. Lee, J. Kim, M. Cho, F. Miao, Y. Yang, H. N. Jung, M. Flavin, H. Liu, G. W. Kong, K. J. Yu, S. I. Rhee, J. Chung, B. Kim, J. W. Kwak, M. H. Yun, J. Y. Kim, Y. M. Song, U. Paik, Y. Zhang, Y. Huang and J. A. Rogers, *Nat. Commun.*, 2015, **6**, 6566.
111 J. Liu and Y. Zhang, *Soft Matter*, 2018, **14**, 693–703.

112 S. Xu, Y. Zhang, J. Cho, J. Lee, X. Huang, L. Jia, J. A. Fan, Y. Su, J. Su, H. Zhang, H. Cheng, B. Lu, C. Yu, C. Chuang, T. I. Kim, T. Song, K. Shigeta, S. Kang, C. Dagdeviren, I. Petrov, P. V. Braun, Y. Huang, U. Paik and J. A. Rogers, *Nat. Commun.*, 2013, **4**, 1543.
113 J. Kim, M. Lee, H. J. Shim, R. Ghaffari, H. R. Cho, D. Son, Y. H. Jung, M. Soh, C. Choi, S. Jung, K. Chu, D. Jeon, S. T. Lee, J. H. Kim, S. H. Choi, T. Hyeon and D. H. Kim, *Nat. Commun.*, 2014, **5**, 5747.
114 S. Xu, Z. Yan, K.-I. Jang, W. Huang, H. Fu, J. Kim, Z. Wei, M. Flavin, J. McCracken, R. Wang, A. Badea, Y. Liu, D. Xiao, G. Zhou, J. Lee, H. U. Chung, H. Cheng, W. Ren, A. Banks, X. Li, U. Paik, R. G. Nuzzo, Y. Huang, Y. Zhang and J. A. Rogers, *Science*, 2015, **347**, 154–159.
115 Z. Wang, F. Yan, Z. Yu, H. Cao, Z. Ma, Z. YeErKenTai, Z. Li, Y. Han and Z. Zhu, *ACS Sens.*, 2024, **9**, 1447–1457.
116 S. Baik, J. Kim, H. J. Lee, T. H. Lee and C. Pang, *Adv. Sci.*, 2018, **5**, 1800100.
117 Y. Song, H. Chen, Z. Su, X. Chen, L. Miao, J. Zhang, X. Cheng and H. Zhang, *Small*, 2017, **13**, 1702091.
118 C. L. Choong, M. B. Shim, B. S. Lee, S. Jeon, D. S. Ko, T. H. Kang, J. Bae, S. H. Lee, K. E. Byun, J. Im, Y. J. Jeong, C. E. Park, J. J. Park and U. I. Chung, *Adv. Mater.*, 2014, **26**, 3451–3458.
119 S. Wang, J. Song, D.-H. Kim, Y. Huang and J. A. Rogers, *Appl. Phys. Lett.*, 2008, **93**, 023126.
120 M. Ha, S. Lim, S. Cho, Y. Lee, S. Na, C. Baig and H. Ko, *ACS Nano*, 2018, **12**, 3964–3974.
121 S. A. Zirbel, R. J. Lang, M. W. Thomson, D. A. Sigel, P. E. Walkemeyer, B. P. Trease, S. P. Magleby and L. L. Howell, *J. Mech. Des.*, 2013, **135**, 111005.
122 S. J. P. Callens and A. A. Zadpoor, *Mater. Today*, 2018, **21**, 241–264.
123 R. Zhao, S. Lin, H. Yuk and X. Zhao, *Soft Matter*, 2018, **14**, 2515–2525.
124 S. H. Sunwoo, K. H. Ha, S. Lee, N. Lu and D. H. Kim, *Annu. Rev. Chem. Biomol. Eng.*, 2021, **12**, 359–391.
125 G. Liu, C. Xu, J. Ren, Y. Liu, L. Yao, Y. Xie, T. Zhang and Y. Liu, *J. Mater. Sci.: Mater. Electron.*, 2023, **34**, 1254.
126 H. Li, Y. Xu, X. Li, Y. Chen, Y. Jiang, C. Zhang, B. Lu, J. Wang, Y. Ma, Y. Chen, Y. Huang, M. Ding, H. Su, G. Song, Y. Luo and X. Feng, *Adv. Healthcare Mater.*, 2017, **6**, 1601013.
127 Y. Wang, X. Li, S. Fan, X. Feng, K. Cao, Q. Ge, L. Gao and Y. Lu, *ACS Appl. Mater. Interfaces*, 2021, **13**, 8901–8908.
128 Y. Wang, D. Li, L. Chao, T. Niu, Y. Chen and W. Huang, *Appl. Mater. Today*, 2022, **28**, 101509.
129 T. Young, *Philos. Trans. R. Soc. London*, 1805, **95**, 65–87.
130 R. N. Wenzel, *Ind. Eng. Chem.*, 1936, **28**, 988–994.
131 A. B. D. Cassie and S. Baxter, *Trans. Faraday Soc.*, 1944, **40**, 546–551.
132 M.-H. Kim, H. Kim, K.-S. Lee and D. R. Kim, *Energy Convers. Manage.*, 2017, **138**, 1–11.
133 H. Gao, Y. Liu, G. Wang, S. Li, Z. Han and L. Ren, *Appl. Surf. Sci.*, 2020, **519**, 146052.
134 E. Arzt, H. Quan, R. M. McMeeking and R. Hensel, *Prog. Mater. Sci.*, 2021, **120**, 100823.
135 X. Wang, C. Fu, C. Zhang, Z. Qiu and B. Wang, *Materials*, 2022, **15**, 4747.
136 X. Wang, H. Jiang, Y. Liu, J. Xu, D. Shan and B. Guo, *Appl. Therm. Eng.*, 2024, **243**, 122515.
137 M. Sala de Medeiros, D. Chanci and R. V. Martinez, *Nano Energy*, 2020, **78**, 105301.
138 L. Lao, D. Shou, Y. S. Wu and J. T. Fan, *Sci. Adv.*, 2020, **6**, eaaz0013.
139 C. Zhou, Y. Li, H. Li, X. Zeng, P. Pi, X. Wen, S. Xu and J. Cheng, *Surf. Coat. Technol.*, 2017, **313**, 55–62.
140 Z. Chen, X. Lu, H. Wang, J. Chang, D. Wang, W. Wang, S. W. Ng, M. Rong, P. Li, Q. Huang, Z. Gan, J. Zhong, W. D. Li and Z. Zheng, *Adv. Mater.*, 2023, **35**, 2210778.
141 F. Wen, Z. Sun, T. He, Q. Shi, M. Zhu, Z. Zhang, L. Li, T. Zhang and C. Lee, *Adv. Sci.*, 2020, **7**, 2000261.
142 C. Pan, K. Kumar, J. Li, E. J. Markvicka, P. R. Herman and C. Majidi, *Adv. Mater.*, 2018, **30**, 1706937.
143 C. Ye, D. Liu, X. Peng, Y. Jiang, R. Cheng, C. Ning, F. Sheng, Y. Zhang, K. Dong and Z. L. Wang, *ACS Nano*, 2021, **15**, 18172–18181.
144 J. Zhao, W. Zhu, X. Wang, L. Liu, J. Yu and B. Ding, *ACS Nano*, 2020, **14**, 1045–1054.
145 M. Cheng, Y. Liu, B. Zhong, H. Wang, Y. Liu, X. Liang, W. Chen, S. Chen, M. Li, W. Xia and X. Wang, *Adv. Mater. Interfaces*, 2019, **6**, 1901178.
146 Z. Ren, Q. Zheng, H. Wang, H. Guo, L. Miao, J. Wan, C. Xu, S. Cheng and H. Zhang, *Nano Energy*, 2020, **67**, 104243.
147 Q. Zhou, K. Lee, K. N. Kim, J. G. Park, J. Pan, J. Bae, J. M. Baik and T. Kim, *Nano Energy*, 2019, **57**, 903–910.
148 M. J. Bathaei, R. Singh, H. Mirzajani, E. Istif, M. J. Akhtar, T. Abbasiasl and L. Beker, *Adv. Mater.*, 2023, **35**, 2207081.
149 W. Yang, X. Cheng, Z. Guo, Q. Sun, J. Wang and C. Wang, *J. Mater. Chem. C*, 2023, **11**, 406–425.
150 L. Upadhyaya, X. Qian and S. Ranil Wickramasinghe, *Curr. Opin. Chem. Eng.*, 2018, **20**, 13–18.
151 J. Dong, Y. Peng, D. Wang, L. Li, C. Zhang, F. Lai, G. He, X. Zhao, X. P. Yan, P. Ma, J. Hofkens, Y. Huang and T. Liu, *Small*, 2023, **19**, 2206572.
152 X. Wang, M. Li, G. Feng and M. Ge, *Appl. Phys. A: Mater. Sci. Process.*, 2020, **126**, 184.
153 W.-l Zhou, T. Wu, Y. Du, X.-h Zhang, X.-c Chen, J.-b Li, H. Xie and J.-p Qu, *Chem. Eng. J.*, 2023, **453**, 139784.
154 C. Xiao, H. Zhang, H. Zhao, H. Xu, J. Huang and T. Zhou, *Appl. Surf. Sci.*, 2022, **605**, 154746.
155 C. Chen, K. Lin, M. Wu, Y. Wang, C. Gao, L. Jia, R. Liu and G. Shan, *Chem. Eng. J.*, 2022, **445**, 136810.
156 R. Zhang, J. Yang, X. Zhao, H. Yang, H. Li, B. Ji, G. Zhou, X. Ma and D. Yang, *ChemCatChem*, 2022, **14**, e202101653.
157 T. Liu, P. Tao, X. Wang, H. Wang, M. He, Q. Wang, H. Cui, J. Wang, Y. Tang, J. Tang, N. Huang, C. Kuang, H. Xu and X. He, *Nat. Nanotechnol.*, 2024, **19**, 51–57.
158 Y. Hou, L. Yu, W. Xie, L. C. Camacho, M. Zhang, Z. Chu, Q. Wei and R. Haag, *Nano Lett.*, 2020, **20**, 748–757.

159 S. Sunderlal Singh and G. L. Samuel, *Opt. Laser Technol.*, 2024, **170**, 110214.
160 E. D. Patamia, N. A. Ostrovsky-Snider and A. R. Murphy, *ACS Appl. Mater. Interfaces*, 2019, **11**, 33612–33619.
161 D. A. Kwon, S. Lee, C. Y. Kim, I. Kang, S. Park and J.-W. Jeong, *Sci. Adv.*, 2024, **10**, eadn1186.
162 P. He, J. Cao, H. Ding, C. Liu, J. Neilson, Z. Li, I. A. Kinloch and B. Derby, *ACS Appl. Mater. Interfaces*, 2019, **11**, 32225–32234.
163 W. Yang, N.-W. Li, S. Zhao, Z. Yuan, J. Wang, X. Du, B. Wang, R. Cao, X. Li, W. Xu, Z. L. Wang and C. Li, *Adv. Mater. Technol.*, 2018, **3**, 1700241.
164 M. Liu, S. Wang, Z. Xiong, Z. Zheng, N. Ma, L. Li, Q. Gao, C. Ge, Y. Wang and T. Zhang, *Biosens. Bioelectron.*, 2023, **237**, 115504.
165 Y. Zhang, S. Zhang, F. Sun, Q. Ji, J. Xu, B. Yao, Z. Sun, T. Liu, G. Hao, Y. Hu, G. Zhang, W. Jiang and J. Fu, *Adv. Funct. Mater.*, 2023, **33**, 2304653.
166 S. Roh, Y. Jang, J. Yoo and H. Seong, *Biochip J.*, 2023, **17**, 174–191.
167 S. Cheng, Z. Lou, L. Zhang, H. Guo, Z. Wang, C. Guo, K. Fukuda, S. Ma, G. Wang, T. Someya, H. M. Cheng and X. Xu, *Adv. Mater.*, 2023, **35**, 2206793.
168 H. Ding, G. Lv, Z. Shi, D. Cheng, Y. Xie, Y. Huang, L. Yin, J. Yang, Y. Wang and X. Sheng, *Nano Res.*, 2021, **14**, 3208–3213.
169 S. Singh, S. Kumar and V. Khanna, *Mater. Today: Proc.*, 2023, DOI: **10.1016/j.matpr.2023.01.010**.
170 S. K. Nemani, R. K. Annavarapu, B. Mohammadian, A. Raiyan, J. Heil, M. A. Haque, A. Abdelaal and H. Sojoudi, *Adv. Mater. Interfaces*, 2018, **5**, 1801247.
171 P. Tan, H. Wang, F. Xiao, X. Lu, W. Shang, X. Deng, H. Song, Z. Xu, J. Cao, T. Gan, B. Wang and X. Zhou, *Nat. Commun.*, 2022, **13**, 358.
172 M. Lin, Z. Zheng, L. Yang, M. Luo, L. Fu, B. Lin and C. Xu, *Adv. Mater.*, 2022, **34**, 2107309.
173 J. Zhu, Y. Xiao, X. Zhang, Y. Tong, J. Li, K. Meng, Y. Zhang, J. Li, C. Xing, S. Zhang, B. Bao, H. Yang, M. Gao, T. Pan, S. Liu, F. Lorestani, H. Cheng and Y. Lin, *Adv. Mater.*, 2024, **36**, 2400236.
174 K. Kwon, J. U. Kim, Y. Deng, S. R. Krishnan, J. Choi, H. Jang, K. Lee, C.-J. Su, I. Yoo, Y. Wu, L. Lipschultz, J.-H. Kim, T. S. Chung, D. Wu, Y. Park, T.-I. Kim, R. Ghaffari, S. Lee, Y. Huang and J. A. Rogers, *Nat. Electron.*, 2021, **4**, 302–312.
175 Z. Zhang, J. Yang, H. Wang, C. Wang, Y. Gu, Y. Xu, S. Lee, T. Yokota, H. Haick, T. Someya and Y. Wang, *Sci. Adv.*, 2024, **10**, eadj5389.
176 C. Yang, H. Zhang, Y. Liu, Z. Yu, X. Wei and Y. Hu, *Adv. Sci.*, 2018, **5**, 1801070.
177 H. Xu, W. Zheng, Y. Zhang, D. Zhao, L. Wang, Y. Zhao, W. Wang, Y. Yuan, J. Zhang, Z. Huo, Y. Wang, N. Zhao, Y. Qin, K. Liu, R. Xi, G. Chen, H. Zhang, C. Tang, J. Yan, Q. Ge, H. Cheng, Y. Lu and L. Gao, *Nat. Commun.*, 2023, **14**, 7769.
178 C. Wei, W. Lin, L. Wang, Z. Cao, Z. Huang, Q. Liao, Z. Guo, Y. Su, Y. Zheng, X. Liao and Z. Chen, *Nano-Micro Lett.*, 2023, **15**, 199.
179 S. Baik, D. W. Kim, Y. Park, T.-J. Lee, S. Ho Bhang and C. Pang, *Nature*, 2017, **546**, 396–400.
180 M. Sala de Medeiros, D. Goswami, D. Chanci, C. Moreno and R. V. Martinez, *Nano Energy*, 2021, **87**, 106155.
181 X. He, C. Fan, T. Xu and X. Zhang, *Nano Lett.*, 2021, **21**, 8880–8887.
182 B. Dai, K. Li, L. Shi, X. Wan, X. Liu, F. Zhang, L. Jiang and S. Wang, *Adv. Mater.*, 2019, **31**, 1904113.
183 J. Park, J. Kim, S.-Y. Kim, W. H. Cheong, J. Jang, Y.-G. Park, K. Na, Y.-T. Kim, J. H. Heo, C. Y. Lee, J. H. Lee, F. Bien and J.-U. Park, *Sci. Adv.*, 2018, **4**, eaap9841.
184 P. Chen, W. Zhang, X. Fan, X. Shi, Y. Jiang, L. Yan, H. Li, C. Wang, L. Han, X. Lu and C. Ou, *Nano Today*, 2024, **55**, 102157.
185 T. Xiao, Z. Zhou, F. Zheng, Y. Zhou, F. Xu, S. Zhang, Z. Shi, Y. Mao and T. H. Tao, *Ultra-Thin, Ultra-Conformal Neural Interfaces*, Vancouver, BC, Canada, 2020.
186 L. Shi, X. Liu, W. Wang, L. Jiang and S. Wang, *Adv. Mater.*, 2019, **31**, 1804187.
187 S. T. Frey, A. B. M. T. Haque, R. Tutika, E. V. Krotz, C. Lee, C. B. Haverkamp, E. J. Markvicka and M. D. Bartlett, *Sci. Adv.*, 2022, **8**, eabq1905.
188 J. Wang, Q. Zhou, A. Wang, Z. Zhu, K. Moses, T. Wang, P. Li and W. Huang, *Adv. Funct. Mater.*, 2024, **34**, 2309704.